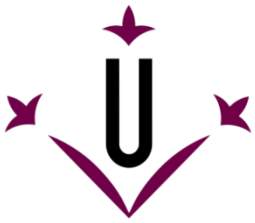



# Recent loss of sensitivity to summer temperature constrains tree growth synchrony among boreal Eurasian forests

T. A. Shestakova[a,b,*], E. Gutiérrez[c], C. Valeriano[c], E. Lapshina[d], J. Voltas[a]

[a] Department of Crop and Forest Sciences—AGROTECNIO Center, University of Lleida, Avda. Rovira Roure 191, 25198 Lleida, Spain

[b] Sukachev Institute of Forest, Akademgorodok 50/28, 660036 Krasnoyarsk, Russia

[c] Department of Evolutionary Biology, Ecology and Environmental Sciences, University of Barcelona, Avda. Diagonal 643, 08028 Barcelona, Spain

[d] UNESCO Chair of Environmental Dynamics and Climate Change, Yugra State University, St. Chekhova 16, 628012 Khanty-Mansiysk, Russia

* Corresponding author:
Tatiana A. Shestakova
Department of Crop and Forest Sciences – AGROTECNIO Center
ETSEA-University of Lleida
Avda. Alcalde Rovira Roure 191
E-25198 Lleida, Spain
tel. +34 973 702855
e-mail: tasha.work24@gmail.com

**Abstract**

High-latitude terrestrial ecosystems are crucial to the global climate system and its regulation by vegetation. Since productivity of boreal forests is much limited by low summer temperatures, it is expected that trees subjected to warming are progressively decreasing their regional growth coherence in the last decades. In this study, we used a comprehensive network of indexed ring-width records to assess 20$^{th}$-century spatiotemporal patterns of climatic sensitivity of forest growth around the Urals mountain range above 60°N (*ca.* 750,000 km$^2$). This area offers an excellent opportunity to test for warming effects as most north Eurasian conifers (including *Larix, Picea* and *Pinus* species) are found along a north-to-south temperature gradient across contrasting soil hydrothermal regimes (permafrost and permafrost-free). We observed positive associations between indexed ring-width and summer temperature over the past century, decreasing southwards. However, weaker (permafrost) or non-significant (permafrost-free) relationships were consistently found at the local and regional scales after 1960. A cointegration analysis indicated that tree-growth release from cold limitation significantly reduced the degree and spatial extent of synchronous growth at short- (annual) and long-term (decadal) scales, most likely by exposing forests to endogenous (local) factors (e.g., competition, soil properties, nutrient availability) and species-specific reactions. Whereas the loss of temperature sensitivity progressively reduced non-permafrost synchrony by 50% over the whole 20$^{th}$ century, permafrost forests decreased their synchrony only after the 1960s, by 20%. Radial growth was enhanced in permafrost sites, as suggested by increasing basal area increment. Our results unequivocally link a substantial decrease in temporal coherence of forest productivity in boreal ecosystems to a growth release from cold limitation that is concurrent with regional warming trends. This emerging pattern points to increasing dependence on local drivers of the carbon balance and the role as carbon sinks of forests in the northern Ural region.

## Highlights

- Regional growth coherence was quantified in a tree-ring network around the Urals
- $20^{th}$-century positive growth-temperature relations were found decreasing southwards
- Weaker or non-significant relationships were consistently found after 1960
- Warming diminished the degree and spatial extent of synchronous growth
- Non-permafrost and permafrost forest growth synchrony was reduced by 50% and 20%

**Keywords:** climate warming, cointegration, conifer species, network coherence, permafrost, tree rings

## Abbreviations

$\hat{a}_C$ – spatial synchrony

BAI – Basal Area Increment

EPS – Expressed Population Signal

*Rbar* – Mean inter-series correlation

$TRW_i$ – indexed Tree-Ring Width

## 1. Introduction

Estimation of tree growth dynamics and its attribution to climate factors across broad scales is highly pertinent for the forecasting of the global ecological impacts of climate change. In boreal forests, summer temperature exerts a positive effect on tree growth increasing northwards that is concurrent with a decrease in sensitivity to precipitation (Vaganov et al., 1999; Kirdyanov et al., 2003; Knorre et al., 2006; Agafonov and Gurskaya, 2013). However, the evidence of a contemporary uncoupling between tree-ring records and temperature in northern latitudes has raised concerns regarding the applicability of dendrochronological approaches to interpret long-term changes in forest productivity and performance (Jacoby and D'Arrigo, 1995; Briffa et al., 1998; Vaganov et al., 1999; Girardin et al., 2016; Allen et al., 2018). The physiographic boundary between Europe and Asia seems not to have been spared from the weakening of the association between radial growth and temperature observed in cold-limited ecosystems (Briffa et al., 1998; Jacoby et al., 2000) (but see Esper et al., 2010) despite the presence of a permafrost layer exacerbating tree productivity's dependence on air temperature above 65°N (Nikolaev et al., 2009).

Regionally correlated climatic forces often synchronize growth among disjunct forests (e.g., climatic teleconnections or spatial synchrony) (Trouet et al., 2012; St. George, 2014; Shestakova et al., 2016, 2018). However, as recently underlined by Allen et al. (2018), much greater emphasis has traditionally been placed on ascertaining the relationship between tree rings and climate for stability at a local rather than broader (regional) scales (as is also the case with boreal forests) (but see e.g., Girardin et al., 2016; Anchukaitis et al., 2017; Ols et al., 2018a, 2018b). Assuming that forest productivity is mainly limited by temperature in high-latitude ecosystems, it is reasonable to expect that trees subjected to warming will progressively decrease their regional growth coherence (Ponocná et al., 2018). This effect should be accompanied by a weakening in tree-growth sensitivity to summer temperature at

88 an interannual scale, which would suggest an increasing role of endogenous (local and
89 taxonomic) imprints on forest carbon dynamics. Yet analysis of tree-ring networks has shown
90 that forest responses to climate warming greatly vary across the boreal biome (Hellmann et
91 al., 2016; Lloyd et al., 2011). For example, shifts in temperature sensitivity associated with
92 warmer springs (related to e.g., an earlier dormancy breaking) or increased temperature
93 variability (related to e.g., a larger impact of climate extremes) may overcome this pattern by
94 enhancing regional growth synchrony, as observed for Central Siberia at the turn of this
95 century (Shestakova et al., 2016). Indeed, understanding long-term synchrony patterns of tree
96 growth becomes highly pertinent to identifying broad-scale emerging threats on forests and
97 threshold tree responses to climate change (Shestakova et al., 2018).

98 In this study, we analyze 20$^{th}$-century changes (temporal instability) in climate-growth
99 associations for a comprehensive tree-ring network surrounding the Arctic, Sub-Arctic and
100 Northern Ural Mountains, and comprising most conifers found in Northern Eurasia. We
101 attempt to relate potential shifts in these associations to changes in the temporal coherence of
102 ring-width records in the high-frequency domain (spatial synchrony). We hypothesized that a
103 decrease in strength of the summer temperature signal in tree-ring chronologies should be
104 paralleled by a regional decrease in spatial synchrony across species and hydrothermal
105 regimes (i.e., permafrost and non-permafrost landscapes), perhaps accompanied by an
106 increase in tree productivity (i.e., release from cold limitation). The tree-ring data were partly
107 gathered from the International Tree-Ring Database (ITRDB; Grissino-Mayer and Fritts,
108 1997) and are comprised of chronologies that consistently cover most of the last century (up
109 to the 1990s). By using updated chronologies (up to 2013) from the eastern side of the Urals,
110 we also evaluated the most recent influence of climate warming on growth dynamics for the
111 area dating back to the early 20$^{th}$ century.

In order to disentangle the relevance of long- and short-term changes in cold-limited growth on the geographical patterns of synchrony in the tree-ring network, we applied a cointegration test of time series analysis (Engle and Granger, 1987). This widespread technique in longitudinal studies enabled us to explicitly integrate stochastic (i.e., non-stationary) trends quantifying the extent of spatial synchrony and temperature-limited tree growth over the 20$^{th}$ century. Cointegration states that if these time series have a functionally dependent relationship, the stochastic trend present in one of the series will be also present in the other (Murray, 1994). The concept of integration guards against the spurious regression problem that arises when linking unrelated stationary variables. Therefore, the main objective of this study was to attain an understanding of the causal relationship between summer temperature – as the main climate driver of tree performance in northern latitudes – and the magnitude of spatial growth coherence among boreal forests at a subcontinental scale. In particular, we aimed to provide inferences regarding the causality of long-term synchrony patterns in radial growth in relation to unstable tree responses to summer temperature. In this way, long-run versus short-run impacts of climate warming were scrutinized for a non-conventional response variable such as spatial synchrony of broad biological relevance to understanding terrestrial ecosystem functioning.

## 2. Materials and methods

### *2.1. Study area*

The study area comprises both sides of the Arctic, Sub-Arctic and Northern Ural Mountains (East Russian Platform and Western Siberia; 60–68°N, 56–68°E) (Fig. 1). It covers an approximate area of 750,000 km$^2$, about half of which is underlain by continuous or discontinuous permafrost extending north and north-east (Fig. 1). The landscape is dominated by low altitude plains separated by the relatively narrow Ural mountain range (up to

137 approximately 150 km wide) following a north-east to south-west direction. Amongst these
138 lowlands, the eastern Western Siberian plain is the most bogged region of the world; in some
139 parts, up to 70–80% is covered by mires (Kirpotin et al., 2009). Forest covers about 36% of
140 this region (Sedykh, 1996).
141

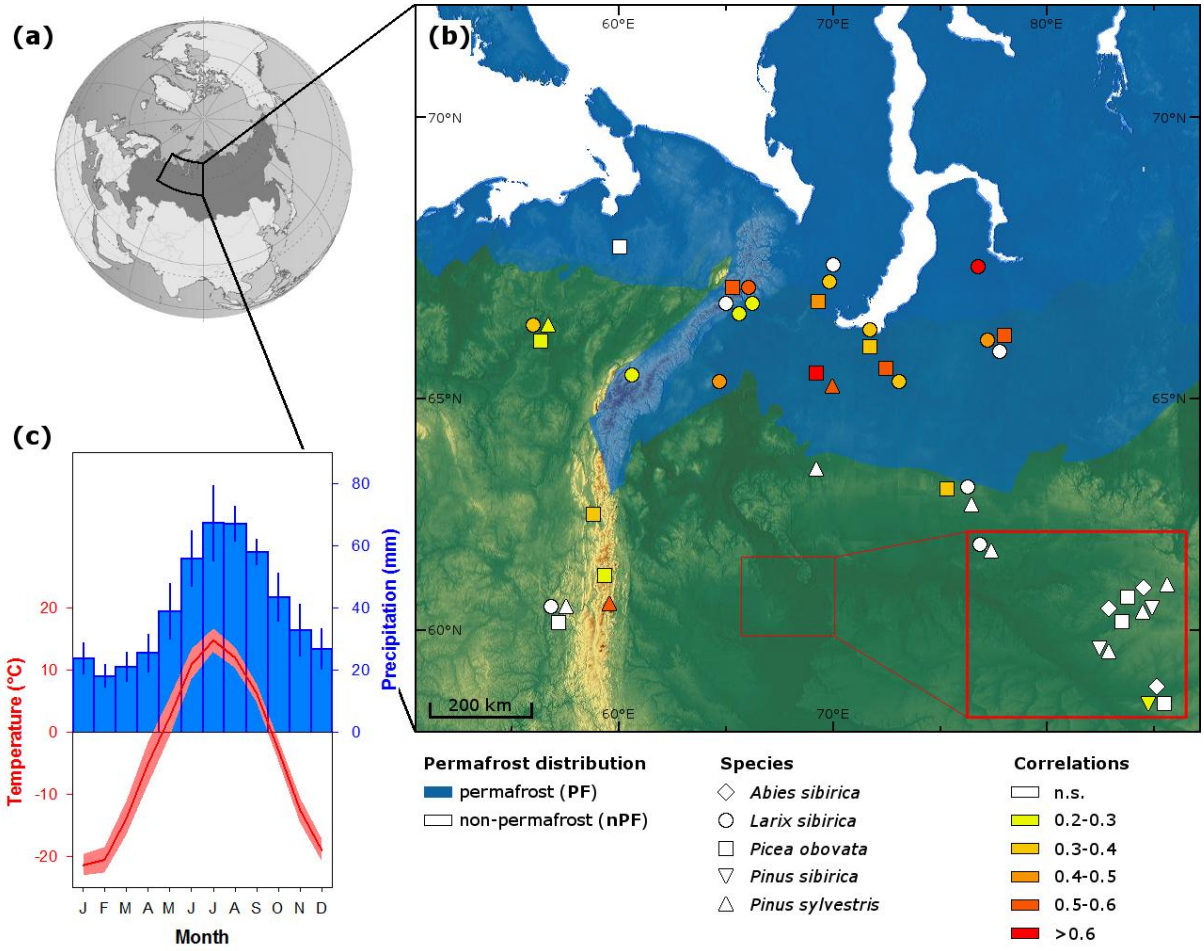

142

143 **Figure 1 (online colour only) (2 column fitting)**

144 **Figure 1.** Geographical distribution and climatic characteristics of the sampling sites in
145 boreal transcontinental Russia (>60°N). (a) Location of the study area. (b) Distribution of
146 sampling sites. Blue shadow on the background map highlights the area with >50%
147 permafrost extension derived from Brown et al. (2002). Species symbols are as follows:
148 circle, *Larix sibirica*; square, *Picea obovata*; triangle, *Pinus sylvestris*; triangle down, *Pinus*
149 *sibirica*; diamond, *Abies sibirica*. The symbol colour depicts the strength of the growth–

climate associations based on bootstrapped correlations between summer (June–July) temperature and indexed tree-ring chronologies ($TRW_i$) for the period 1911–1990. The climate data are obtained from high-resolution ($0.5° \times 0.5°$) CRU TS4.01 dataset (Harris et al., 2014) at a site level. Non-significant correlations ($P > 0.05$) are shown with white symbols. (c) Climate diagram corresponding to the study area. The primary *y*-axis indicates monthly mean temperature (lines), and the secondary *y*-axis monthly precipitation (bars). Average monthly values of climate factors are estimated based on the CRU data from each site for the period 1911–2013. The standard errors of the estimates are shown as shaded area (temperature) and error bars (precipitation).

The climate is continental with a prolonged cold season, large intra-annual temperature fluctuations and moderate precipitation (Fig. 1). The mean annual temperature for the area is –3.8°C, with January being the coldest (–21.2°C) and July the warmest month (+15.0°C) (reference period: 1911 to 2013, CRU TS 4.01 dataset; Harris et al., 2014). However, the areas west of the Urals are 1–2°C warmer in winter than the eastern floodplains of Western Siberia because the latter are chilled by Siberian air masses whereas the former are warmed by Atlantic winds. This implies that the boundary between permafrost (PF) and non-permafrost (nPF) zones occurs from northwest to southeast at ~65°N (Fig. 1). The transition to above-zero mean daily temperatures occurs progressively during the second half of May northwardly and to below-zero temperatures from late September through early October southwardly. The snow cover is formed in October and lies for about seven months. The mean annual precipitation is 490 mm, with about 60% occurring during the warm period (May–September) as rain events.

Three main vegetation types (forest tundra, northern taiga and middle taiga) are found following the north-to-south temperature gradient, with conifers the dominant species

(Tchebakova et al., 1994). *Larix sibirica* (Siberian larch) is the northernmost conifer, which dominates in the forest tundra zones of continuous permafrost with an admixture of *Picea obovata* (Siberian spruce). The northern taiga, mainly underlain by discontinuous permafrost, is co-dominated by larch-spruce forest, while the non-permafrost middle taiga is dominated by *Pinus sibirica* (Siberian pine), *P. obovata* and, to a lesser extent, by *L. sibirica*. *Pinus sylvestris* (Scots pine) and *Abies sibirica* (Siberian fir) are sparse and can be found mainly in the southern part of the study area, at their northernmost distribution limit. Out of the eight conifers that are found across the vast territory of Siberia, only three, which belong to the *Larix* genus, are not included in this work: *L. cajanderii*, *L. gmelinii* and *L. sukaczewi*. The study sites, representative of most forests in the region, range in elevation from 20 to 400 m a.s.l., except for two sites located at 670 and 720 m a.s.l.

*2.2. Ring-width network and data processing*

Fieldwork was conducted in the area of Khanty-Mansiysk (Khanty–Mansi Autonomous Okrug, Russia; hereafter K-M) in July 2014. This middle-taiga region has scarcely been surveyed for dendrochronological studies (Blanchet et al., 2017). The five conifer species were sampled at seven sites according to the presence of each species and separated by a maximum of *ca*. 200 km, resulting in a total of 14 site-species combinations: *A. sibirica* (three sites), *L. sibirica* (one site), *P. obovata* (three sites), *P. sibirica* (three sites) and *P. sylvestris* (four sites) (Fig. 1, Table A.1). 10 to 20 mature, dominant and healthy trees growing on mineral soils (Podzols) were randomly selected per site and species. Trees growing on peat soils (Histosols) were purposely not sampled to avoid the added variability in reactions to climate posed by trees growing on these soils (Blanchet et al., 2017). We targeted undisturbed forests with no visible human (e.g. logging) or natural disturbances (e.g. fire scars, pests). Two cores from the opposite cross-slope sides of the trunk were extracted at

breast height with a 5-mm-diameter increment borer. Samples were oven-dried at 60°C for 48 h and sanded with sandpapers of progressively finer grain until tree rings were clearly visible. Tree rings were visually cross-dated and measured using high-resolution images produced on a flat-bed scanner coupled with WinDendro™ software (Regent Instruments, 2012). Cross-dating was verified with the COFECHA program (Holmes, 1983).

The abovementioned dataset was complemented with annually resolved long-term tree-ring width (TRW) records available from the International Tree-Ring Data Bank (ITRDB; Grissino-Mayer and Fritts, 1997) (Fig. 1). These included *L. sibirica*, *P. obovata* and *P. sylvestris* growing on Gelic Gleysols at permafrost sites, and on Podzols (in lowlands) or Podzoluvisols (in the Urals mountain range) at non-permafrost sites. Altogether, they allowed us to undertake a comprehensive dendrochronological characterization of the lowlands flanking the Ural Mountains above 60°N. A total of 48 site chronologies comprising 14 newly developed chronologies and 34 ITRDB chronologies were used, amounting to 746 trees (Fig. 1, Table A.1). The resulting TRW network contained records from *A. sibirica* (three sites), *Pinus* spp. (13 sites, including three sites of *P. sibirica* and 10 sites of *P. sylvestris*), *P. obovata* (15 sites) and *L. sibirica* (17 sites).

Our analysis mainly focused on high-frequency (i.e., interannual) variability that was potentially related to climate (Cook and Kairiukstis, 1990), disregarding low-frequency (i.e., interdecadal) trends in tree growth at this stage. To this end, the individual series were first standardized using the Friedman supersmoother spline with variable span tweeter sensitivity $\alpha = 5$ (Friedman, 1984). This procedure minimizes the effect of biological trends (e.g., tree age) and disturbances (e.g., fire scars) on radial growth. Standardization converted ring-width measurements into dimensionless indices with a mean value of 1 and constant variance. Next, autoregressive models were applied to remove the first-order temporal autocorrelation in the detrended series and produce residual or pre-whitened indices. Finally, a biweight robust

mean was computed to provide indexed tree-ring width chronologies ($TRW_i$) for each site-species combination. These procedures were conducted using ARSTAN v. 44h2 (Cook and Krusic, 2005). The reliability of ring-width chronologies for capturing the hypothetical population signal was checked against the expressed population signal (*EPS*) criterion with a threshold value of 0.85 (Wigley et al., 1984). Inter-series correlation (*Rbar*) statistics were used to estimate the internal chronology coherence (Wigley et al., 1984).

*2.3. Analysis of spatial variability of tree growth*

The temporal coherence of $TRW_i$ among chronologies was analyzed in order to determine how far common growth patterns extended over the entire region. The study period was most of the 20$^{th}$ century (1911–1990), as most chronologies had *EPS* over 0.85 from 1911 onwards (except for one *A. sibirica* and three *P. sylvestris* chronologies), and the majority of ITRDB chronologies ended during the 1990s (Table A.1). Simple correlation coefficients (*r*) between pairs of chronologies were plotted on the geographic distance between sites, and a Mantel test (Fortin and Gurevitch, 1993) was used to determine the significance of these relationships. Two contrasting spatial patterns of synchronous growth were detected, which approximately matched the presence or absence of permafrost (continuous or discontinuous) in the landscape. These patterns were therefore characterized for each landscape type and modified correlograms were used to aid interpretation of the relationship between synchrony and distance between sampling locations (Koenig and Knops, 1998). In order to achieve this end, the statistical significance of pairwise correlations was calculated within classes located 250 km apart.

Spatial synchrony patterns were further explored through linear mixed-effects models as described in Shestakova et al. (2014, 2018) and Alday et al. (2018). For this purpose, chronologies were grouped *a priori* into potentially (ecologically or ecophysiologically)

250 homogeneous subsets according to membership to either a particular landscape type (i.e.,
251 permafrost [PF] or non-permafrost [nPF]; ~ 65°N boundary) or genus (i.e., *Larix, Picea* or
252 *Pinus*). A number of variance-covariance (VCOV) models accommodating between- and
253 within-group variability were used to characterize the pattern of covariation among the
254 previously-defined groups, which were compared using standard criteria for model selection
255 (Akaike and Bayesian information criteria) (Burnham and Anderson, 2002). The VCOV
256 models tested were broad evaluation (null model ignoring groups), narrow evaluation (lack of
257 common signal between groups) and unstructured (full model with different (co)variances
258 and correlations). Subsequently, estimates of spatial synchrony (or mean inter-chronology
259 correlation, $\hat{a}_C$) were derived using the best VCOV model for chronologies belonging to
260 either the same landscape (genus) or different landscapes (genera) (Shestakova et al., 2018).
261 Values of $\hat{a}_C$ close to 1 indicate near-perfect synchrony among chronologies, while values
262 close to or below 0 denote spatial asynchrony.

263 VCOV structures were first tested over the whole period (1911–1990). Based on this
264 output, the evolution of changes in $\hat{a}_C$ was then studied for successive 30-year segments,
265 lagged by one year. This was done to characterize shifts in common $TRW_i$ variability over
266 time potentially related to instability in the relationship between tree growth and summer
267 temperature at the high-frequency domain (see subsection 2.7). In addition, we evaluated the
268 common signal strength and its temporal stability among the more recent K-M chronologies
269 (1911–2013 period). Significant trends in the evolution of the metric over time were
270 determined using the non-parametric Kendall $\tau$ rank correlation coefficient. We also tested
271 for trend break points (i.e., the points where regression coefficients change) to determine
272 structural changes in a linear regression setup. For this analysis, the minimum segment length
273 was set to 25 years. In case a trend break point was detected, the $\tau$ rank correlation was

calculated over the period after the break point (i.e., corresponding to the most recent trend). Break points were often found corresponding to the year 1959 (see Results section).

*2.4. Development of master chronologies*

We derived aggregated (master) chronologies of radial growth summarizing $TRW_i$ patterns shared by groups of chronologies according to the aforementioned classification strategies, that is, (*i*) landscape-based (PF, nPF) and (*ii*) taxonomic-based (*Larix*, *Picea*, *Pinus*). For this purpose, we used best linear unbiased prediction (BLUP) of year effects based on best fitting VCOV models. BLUP maximizes the correlation between true and predicted values associated with the random (year) effect for the combined analysis of multiple chronologies. The predictors provide relative ring-width indices with a zero-mean (Shestakova et al., 2016). BLUPs were estimated for the period 1911–1990 at both landscape and genus level. We also developed a master chronology for the period 1911–2013 that exclusively involved the set of most recent K-M chronologies. The resulting aggregated (master) chronologies were subsequently used as inputs for climate analyses.

*2.5. Climate analyses*

Long-term series of monthly climate variables (temperature and precipitation) were obtained from the nearest grid point to each sampling site of the high-resolution gridded climate dataset (Climatic Research Unit, CRU TS 4.01; Harris et al., 2014). Bootstrapped correlations between $TRW_i$ chronologies and climate from the previous June to September of the year of tree-ring formation were calculated to assess climate drivers of tree growth. This analysis was performed over the period 1911–1990. The quality of the climate data before 1950 was evaluated by assessing the number of instrumental records contributing to each CRU cell (0.5°×0.5° grid) over the region at any time step. There were up to eight stations

used to produce a climate series for a particular CRU grid cell (Harris et al., 2014). Of the total number of stations available across the study region, 50% covered the entire period used for the climate analysis (i.e., starting from 1911), and >85% of the stations were incorporated to the analysis during the first two decades (1912–1927 period).

*2.6. Evaluation of temporal instability in growth-climate associations*

We refer to temporal instability as a disagreement at the high-frequency (i.e., interannual) domain between $TRW_i$ and summer (June–July) temperature for a sufficiently long period of time (i.e., 2–3 decades). Two approaches were used to check for temporal instability. The first approach explored tree responses to June–July temperature independently for the periods 1911–1959 (pre-break point in synchrony trends) and 1960–1990 (post-break point) using either site chronologies or aggregated (master) chronologies. In this last case, CRU-based averaged June–July temperatures were obtained over each landscape type or genus distribution covered by the network of chronologies in order to produce annually resolved regional climate series. These series were then used to investigate whether growth responsiveness to summer temperature changed between consecutive sub-periods. This procedure used either 'raw' or residual climatic series. The former refers to the monthly climate data 'as it is', whereas the latter originated having removed the linear trend (if present) and first-order autocorrelation. The second approach calculated running correlations between radial growth and June–July temperature for successive 30-year windows and for each landscape type or genus using the corresponding aggregated (master) chronologies. Significant trends in the evolution of the metric over time were determined using Kendall $\tau$ rank correlation coefficient.

323 *2.7. Cointegration analysis: Linking spatial synchrony to unstable temperature responses*

324 Changes in the temporal coherence of indexed ring-width records were examined in
325 relation to shifts in temperature-growth associations. To this end, synchrony ($\hat{a}_C$) estimates
326 and *r*-values quantifying the relationship between June–July temperature and growth were
327 jointly analyzed at landscape type or genus level for successive 30-year segments. We used a
328 cointegration method, which is widely applied in the analysis of economic time series (Engle
329 and Granger, 1987), but seldom in ecology (Brown et al., 2011; but see D'Arrigo et al.,
330 2004). Briefly, two time series that are integrated of order 1, or *I(1)* for short, are said to be
331 co-integrated if a linear combination of them exists that is stationary, or *I(0)*. If two time-
332 related processes co-integrate, they can be considered together as they form equilibrium
333 relationships.

334 Following the Engle–Granger two-step method, let us define $\hat{a}_{Ct}$ and $r_t$ as the running
335 statistics, lagged by one year, of $\hat{a}_C$ and *r* as outlined above. In a univariate context, $\hat{a}_{Ct}$ (or $r_t$)
336 is *I(1)* if its first difference $\Delta\hat{a}_{Ct}$ ($\Delta r_t$) is *I(0)*. If both series are non-stationary and
337 cointegrated, by regressing $\hat{a}_{Ct}$ on $r_t$ we may legitimately obtain a linear combination *I(0)* (or
338 'cointegrating regression model' of the form $\hat{a}_{Ct} = a + br_t + R_t$) that, if present, represents the
339 long-run equilibrating relationship between $\hat{a}_C$ and the extent of growth limitation by summer
340 temperature (*r*). This cointegration relationship is unique as there are only two processes
341 involved in the analysis (Engle and Granger, 1987). Following our main hypothesis, the
342 results from the cointegrating regression model were used to derive a long-run marginal
343 tendency (or slope coefficient b) of synchrony to decrease owing to a warming-induced
344 relaxation of cold-limited growth.

345 Alternatively, an 'error correction model' can be obtained that permits quantification
346 of the short-term dependence of spatial synchrony on temperature-limited growth (Engle and
347 Granger, 1987). This model can be expressed as:

$$\Delta \hat{a}_{Ct} = \alpha_1 + \alpha_2 \Delta r_t + \alpha_3 R_{t-1} + u_t \quad (1)$$

where $R_{t-1}$ refers to the least squares residuals series (lagged one year) from the 'cointegrating regression model' above and $u_t$ is a residual term. The coefficient $\alpha_2$ quantifies the short-run dynamics of the relationship between $\hat{a}_{Ct}$ and $r_t$. In turn, the coefficient $\alpha_3$ is expected to be negative and significant if synchrony and cold-limited growth co-integrate. Extended details regarding cointegration methods can be found in Kirchgässner and Wolters (2007).

In practical terms, the approach involved three steps:

(i) Test the series unit root, *I(1)*, for $\hat{a}_{Ct}$ and $r_t$ independently by applying the augmented Dickey-Fuller (ADF) test and allowing for either the presence of *drift* or *drift + trend* in the time series. Two statistics were obtained: the ADF $\tau$ statistic (D-F's $\tau$) and the normalized bias $\rho$ statistic. Both test the null hypothesis $I = 1$. If $H_0$ (there is unit root) could not be rejected, then we proceeded with the next step.

(ii) Check whether $R_t$ is stationary *I(0)* with D-F's $\tau$ and, if affirmative, then $\hat{a}_{Ct}$ and $r_t$ are co-integrated (Engle-Granger co-integration test; Engle and Granger, 1987).

(iii) Obtain the cointegrating regression model (for long-run equilibrium) and the error correction model (for short-term dynamics) as defined above through ordinary least squares regression.

This procedure was independently applied to each landscape type (PF, nPF) and genus (*Larix*, *Picea*, *Pinus*), and also to K-M chronologies containing updated ring-width records. It was also evaluated over the period 1960–1990 for PF because a break point in $\hat{a}_{Ct}$ values was detected in 1959, implying a change in synchrony trend. A flowchart of the different steps followed to implement the cointegration analysis is presented in Figure A.1.

371 *2.8. Long-term changes in basal area increment*

372 We also explored low-frequency trends in radial growth to investigate 20$^{th}$-century
373 shifts in forest productivity. For each site-species combination, raw (absolute) tree-ring width
374 measurements were transformed to basal area increment (BAI, cm$^2$ year$^{-1}$). BAI represents an
375 accurate indicator of tree vigor and absolute growth over time because it accounts for the
376 variation caused by adding volume to a circular stem (Biondi and Qeadan, 2008). It relies
377 upon the assumption of near-perfect circular and centered trunk sections. BAI was calculated
378 from the set of cross-dated tree-ring width series according to:

$$BAI = \pi(R_t^2 - R_{t-1}^2), \quad (2)$$

379 where $R$ is the radius of the tree and $t$ is the year of tree-ring formation. Finally, we calculated
380 biweight means of yearly BAI values for each site-species combination.

381 To check for age-independent absolute growth trends, BAI data were subjected to a
382 linear mixed-effects model for old-growth trees (>200 years) exclusively (481 out of 746
383 trees). This approach minimizes the transitory dynamics associated with stand development
384 and succession. The following effects were included in the model: *group* (using either
385 landscape or genus classification), *period* (pre-break point [1911–1959], post-break point
386 [1960–1990]), *chronology* nested to *group*, *year* nested to *period*, and the interaction between
387 *group* and *period*. The terms *group* and *period* and its interaction were introduced as fixed
388 effects, and *chronology* and *year* as random effects. BAI data were log-transformed prior to
389 analysis in order to meet the assumption of homogeneity of residual variances.

390 The MIXED procedure of SAS/STAT software (ver. 9.4, SAS Inc., Cary, NC, USA)
391 was used for the investigation of BAI records, and the R package 'DendroSync' ver. 0.1.0 (R
392 Foundation for Statistical Computing, Vienna, Austria) (Alday et al., 2018) was used for the
393 analysis of synchrony. In both cases, the restricted maximum likelihood (REML) algorithm
394 was used to estimate model parameters. The non-centered correlogram function (correlog.nc)

implemented in the R package 'ncf' ver. 1.1-5 was used to carry out spatial autocorrelation analysis. The R package 'strucchange' ver. 1.5-1 (Zeileis et al., 2002) was used to determine the trend break points in synchrony. The temporal relationships with climate were assessed using 'treeclim' ver. 2.0.0 in R software (Zang and Biondi, 2015). Simple correlations were considered significant at $P < 0.05$. Finally, the cointegration analysis was performed using the ARIMA, REG and VARMAX procedures of SAS/STAT.

## 3. Results

### *3.1. Regional climate*

Landscape types differed in climate for the period 1911–2013. Non-permafrost forests (nPF) were warmer and wetter compared to forests growing over permafrost (PF) (mean annual temperature = –2.1°C *vs.* –5.5°C; annual precipitation = 542 mm *vs.* 434 mm). These differences were especially marked for spring (March–May) and summer (June–August) temperature (diff. = +5.3°C and +3.3°C respectively) and summer precipitation (diff. = +45 mm). Despite the regional differences, mean annual temperature increased at a similar rate of ~0.01°C year$^{-1}$ in both landscapes (Fig. A.2a). The warming trend was evident in spring (March, May) and summer (June–July) months. In particular, we found an increase in June–July temperature for the whole 1911–2013 period ($b = 0.01$°C year$^{-1}$), which accelerated from 1950 irrespective of landscape type ($b = 0.02$°C year$^{-1}$) (Fig. A.2c). In addition, the climate became wetter in both landscapes over the period 1911–2013; however, these changes were more pronounced in PF sites ($b = 1.00$ mm year$^{-1}$ *vs.* $b = 0.07$ mm year$^{-1}$ for nPF) (Fig. A.2b). The increase in precipitation was particularly evident during the cold season and spanned from November to January in nPF ($b = 0.24$ mm year$^{-1}$) and from October to April in PF ($b = 0.93$ mm year$^{-1}$) (Fig. A.2d).

420 *3.2. Site-level tree growth*

421 Ring-width chronologies with *EPS*> 0.85 covered the period of 1911–1990, with the
422 exception of four stands sampled in 2014 (Table A.1). The *Rbar* statistics ranged from 0.28
423 (*A. sibirica* 'ABSI3' in nPF) to 0.76 (*L. sibirica* 'LASI12' in PF). We observed a progressive
424 external forcing on growth increasing northwards ($r = 0.62$, $P < 0.001$, for the correlation
425 between *Rbar* and latitude), and consistent differences between PF and nPF (*Rbar* = 0.54 ±
426 0.12 *vs*. 0.41 ± 0.08 respectively; mean ± SE). The distribution of mean ring-width values
427 across the network was also (negatively) related to latitude ($r = –0.72$, $P < 0.001$).
428 Accordingly, site mean radial growth was positively related to summer (June–July)
429 temperature ($r = 0.77$, $P < 0.001$). For old-growth trees, BAI increased in PF sites by 15% in
430 the period 1960–1990 compared with the preceding period. BAI also increased by 31%
431 between the two periods in the case of *Larix*. Conversely, significant changes in BAI were
432 observed neither in nPF sites nor for *Picea* species, whereas BAI decreased by 13% for *Pinus*
433 species (Table A.2).

434 The common growth signal between pairs of chronologies decreased significantly
435 with distance (Fig. 2). However, two distinct spatial patterns were contingent on landscape
436 type. A close relationship between common growth signal and distance was found in PF,
437 where a linear decreasing trend was observed (Fig. 2a). Conversely, a looser exponential
438 decay of common signal with distance was found in nPF (Fig. 2b). The analysis of spatial
439 autocorrelation confirmed that the common signal declined linearly with distance and
440 extended up to 1,000 km in PF (i.e., the approximate maximum site distance in this study)
441 (Fig. 2c). In contrast, a significant spatial autocorrelation was observed only up to 500 km for
442 nPF, with a considerably lower mean correlation for each distance class compared with PF
443 (Fig. 2d).

444

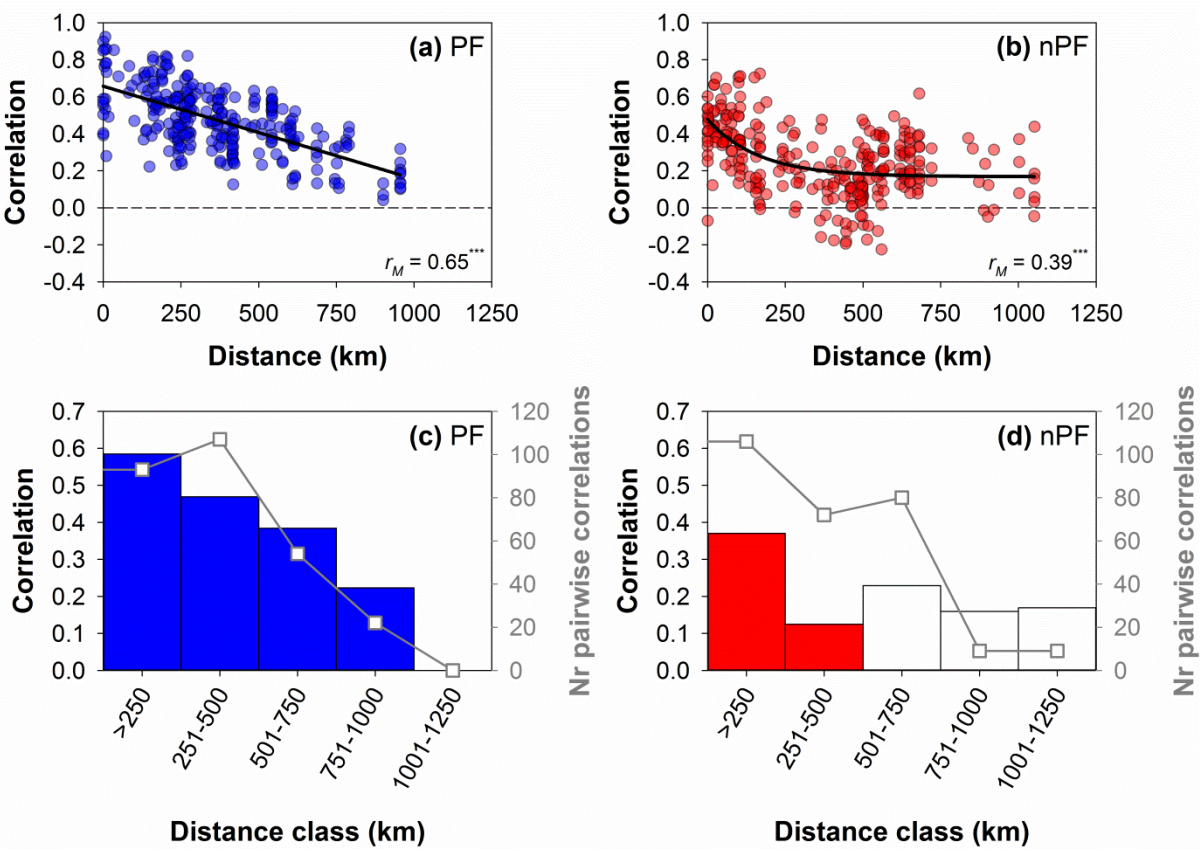


445

446 **Figure 2 (online colour only) (2 column fitting)**

447 **Figure 2.** Spatial patterns of indexed tree-ring chronologies ($TRW_i$) across boreal
448 transcontinental Russia (>60°N) for the period 1911–1990. (a,b) Pairwise correlations of site-
449 level $TRW_i$ as a function of geographical distance across landscape types. The patterns are
450 summarized using a linear function (a; permafrost sites, PF) or a negative exponential
451 function (b; non-permafrost sites, nPF). Asterisks after the correlation coefficient ($r_M$)
452 indicate level of significance based on a Mantel test ($^{***}P < 0.001$). (c,d) Spatial structure of
453 $TRW_i$ across landscape types. The spatial autocorrelation in the tree-ring network was
454 characterized for five consecutive distance classes (listed on the *x*-axis). Mean *r*-values and
455 their statistical significance (*P*) within each distance class were estimated from 1,000
456 randomizations. Filled bars depict significant correlation coefficients ($P < 0.05$). Grey lines
457 represent the number of pairwise correlations in each distance class.

458

459 *3.3. Regional synchrony*

460 The degree of synchronous growth was examined at the group level for each grouping
461 strategy (landscape- and genus-based). In both cases, synchrony was estimated based on an
462 unstructured VCOV model (full model with different (co)variances and correlations), which
463 consistently provided the best goodness-of-fit statistics. For landscape-based grouping,
464 spatial synchrony was twofold higher at PF ($\hat{a}_C = 0.44 \pm 0.04$; mean ± SE) compared with nPF
465 ($\hat{a}_C = 0.22 \pm 0.03$). This difference was unrelated to changes in mean distance between pairs
466 of chronologies across landscapes: 369 ± 14 km for PF (range = 0–956 km) and 380 ± 16 km
467 for nPF (range = 0–1,051 km). Synchrony between chronologies belonging to different
468 landscapes was substantially lower ($\hat{a}_C = 0.14 \pm 0.04$) than that observed within landscapes.

469 For genus-based grouping, the highest synchrony was observed among *Larix*
470 chronologies ($\hat{a}_C = 0.44 \pm 0.04$), followed by *Picea* ($\hat{a}_C = 0.37 \pm 0.04$) and *Pinus*
471 ($\hat{a}_C = 0.30 \pm 0.04$). These results were essentially independent of the mean site distance for
472 each genus (*Larix*: 488 ± 26 km [range = 0–1,234 km]; *Picea*: 567 ± 25 km [range = 0–
473 1,201 km]; and *Pinus*: 493 ± 36 km [range = 0–1,051 km]). At the between-genus level,
474 synchrony was relatively high for *Larix*/*Picea* ($\hat{a}_C = 0.28 \pm 0.04$), but substantially weaker for
475 other combinations (0.15 ± 0.04 for *Picea*/*Pinus* and 0.13 ± 0.04 for *Larix*/*Pinus*).

476

477 *3.4. Temporal changes in regional synchrony*

478 Synchrony decreased during the period 1911–1990 in nPF, but no overall trend was
479 observed in PF or between landscapes (Fig. 3a). However, break points in trends were
480 detected in the two latter cases in 1959, the year after which $\hat{a}_C$ records started to decline. For
481 genus-based grouping, we also found a general decrease in synchrony (Fig. 3b). At the
482 between-genus level, $\hat{a}_C$ between *Picea/Pinus* also diminished over time. In spite of a slightly
483 increasing trend in synchrony detected between *Larix* and either *Picea* or *Pinus* over the

whole period, the recent decades were characterized by a significant decrease in $\hat{a}_C$ (i.e., after 1959) (Fig. 3c). In line with the synchrony reduction observed in nPF, we also found a steady $\hat{a}_C$ decrease in K-M over the period 1911–2013 (Fig. A.3a). On the other hand, there were distinct trajectories in $\hat{a}_C$ at the genus level in K-M, with *Abies* showing a decreasing trend, *Picea* an increasing trend, and *Pinus* showing no change (Fig. A.3b). All pairwise combinations among genera showed a robust $\hat{a}_C$ decrease over time (Fig. A.3c).

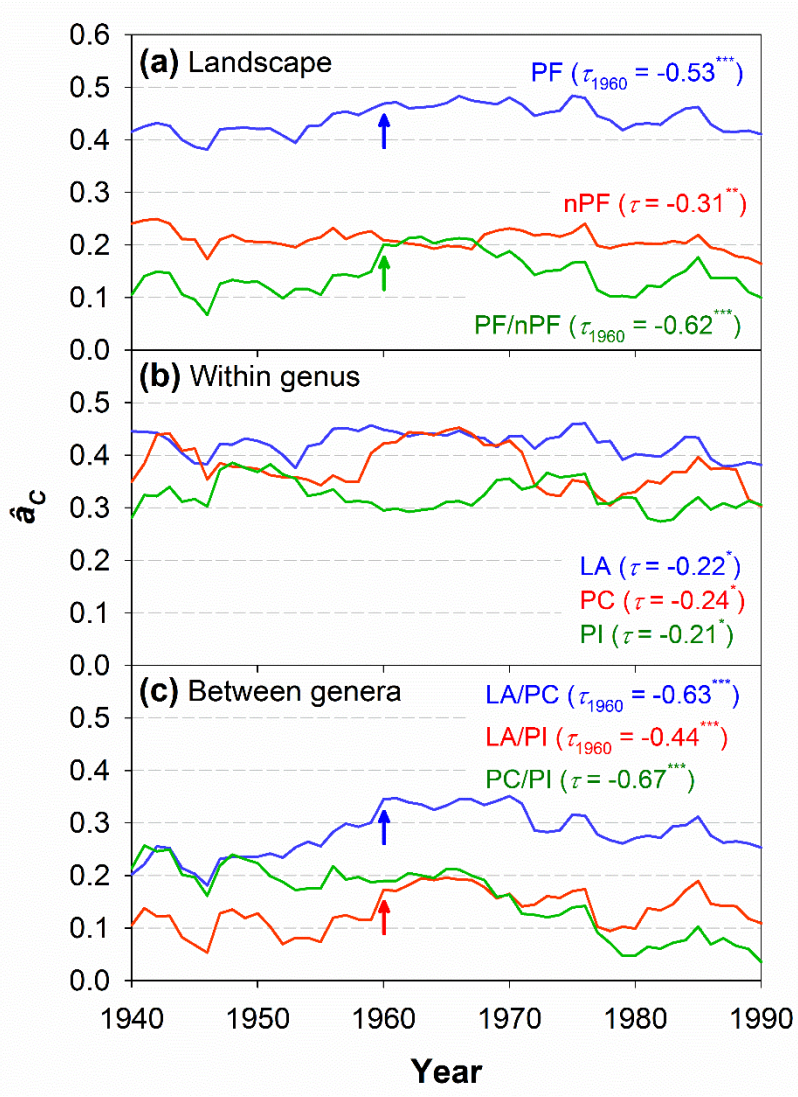


**Figure 3 (online colour only) (1 column fitting)**

**Figure 3.** Temporal changes in spatial synchrony ($\hat{a}_C$) at landscape (a) and genus levels (b, c) for the period 1911–1990. Changes in $\hat{a}_C$ were characterised for successive 30-year segments lagged by one year. Significant trends over time are depicted as Kendall's $\tau$ corresponding to

the whole period or to the period after a breakpoint occurred (indicated with a vertical arrow if present). Asterisks after the $\tau$ values indicate level of significance: $^{*}P < 0.05$; $^{**}P < 0.01$; $^{***}P < 0.001$. Abbreviations: PF, permafrost; nPF, non-permafrost; LA, *Larix sibirica*; PC, *Picea*; PI, *Pinus*.

### *3.5. Climate drivers of tree growth*

Site-level relationships between $TRW_i$ and climate displayed a strong spatial pattern, revealing distinct growth responses between landscapes (Figs. 1 and A.4). As expected, $TRW_i$ was consistently enhanced by current summer (June–July) temperature in PF (i.e., cold-limited growth), with moderate to strong temperature–growth relationships (in most cases $\sim 0.3 < r < 0.6$). In contrast, $TRW_i$ contained miscellaneous climate signals in nPF, positively (but mildly) responding to either summer temperature or precipitation depending on the site (typically $r < 0.3$). As a result, the strength of growth sensitivity to June–July temperature was latitudinally structured increasing northwards ($r^2 = 0.40$, $F$-value after autocorrelation correction = 7.63, $P = 0.008$), as mean summer temperature decreased linearly with latitude ($r = –0.94$, $P < 0.001$). Occasionally, ring width was negatively influenced by warm and/or dry summers (July–August) in the year before tree-ring formation. Growth was also sensitive to out-of-season temperature (mainly previous October, positively) and precipitation (current January–February, negatively), albeit with $|r| < 0.3$. The importance of these variables was limited to particular site-species combinations (Fig. A.4) and, thus, we focused on the current summer temperature response as a common climatic driver across the network in subsequent analyses.

In accordance with the site-level results, landscape-level aggregated $TRW_i$ chronologies also showed significant positive associations with June–July temperature for the period 1911–1990, and growth sensitivity to summer temperature was noticeably stronger for

PF compared with nPF (Fig. A.5). These patterns remained unaltered following the standardization of climate records and removal of autocorrelation (Fig. A.5), so we used 'raw' temperature series for further climate analyses. Similar results were obtained across genera, with the strongest (positive) associations between aggregated chronologies and June–July temperature found for *Larix*, followed by *Picea* and *Pinus* (not shown).

### *3.6. Changes in tree growth responsiveness to summer temperature*

The latitudinal dependence of growth sensitivity to summer temperature decreased in the period 1960–1990 in comparison with the preceding period (Fig. 4a,b). Similar changes in cold-limited growth being dependent on mean summer temperature were also observed (Fig. 4c,d). The number of sites with a significant growth-temperature relationship declined from 57% to 30%. Such a loss of temperature sensitivity was particularly relevant in nPF. While the association between growth and summer temperature gradually weakened after 1960 for PF, as shown by its aggregated chronology (Fig. 5a,c), it completely vanished for nPF (Fig. 5b,d). These results were essentially unrelated to potential ontogenic effects that could have partially driven the observed tree responses to climate (Fig. A.6). At the genus level, *Larix* displayed a pronounced decrease in growth sensitivity to summer temperature, but *Picea* and *Pinus* became insensitive to summer temperature after 1960 (Fig. 6).

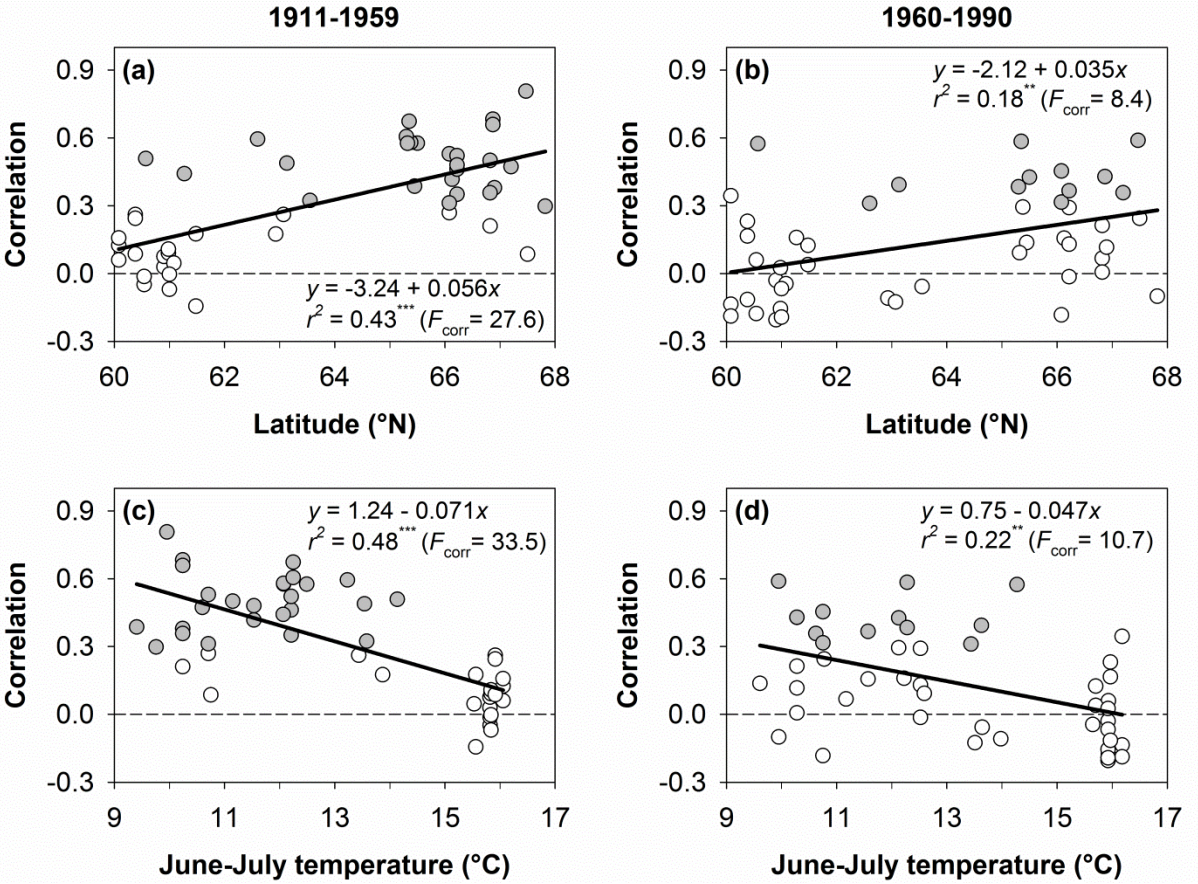


**Figure 4 (2 column fitting)**

**Figure 4.** Relaxation of latitudinal (a,b) and temperature (c,d) responsiveness of indexed tree-ring chronologies ($TRW_i$) to summer temperature for the two halves of the study period: 1911–1959 (*left panels*) and 1960–1990 (*right panels*). Growth–climate associations are calculated based on bootstrapped correlations between summer (June–July) temperature and site-level $TRW_i$. The climate data are obtained from high-resolution ($0.5° \times 0.5°$) CRU TS4.01 dataset (Harris et al., 2014) at a site level. Filled circles correspond to significant correlation coefficients ($P < 0.05$). Significant linear trends ($^{**}P < 0.01$; $^{***}P < 0.001$) across the latitudinal (or temperature) gradient are depicted as black lines after spatial autocorrelation correction using a spherical semivariogram describing the degree of spatial dependence ($F_{corr}$).

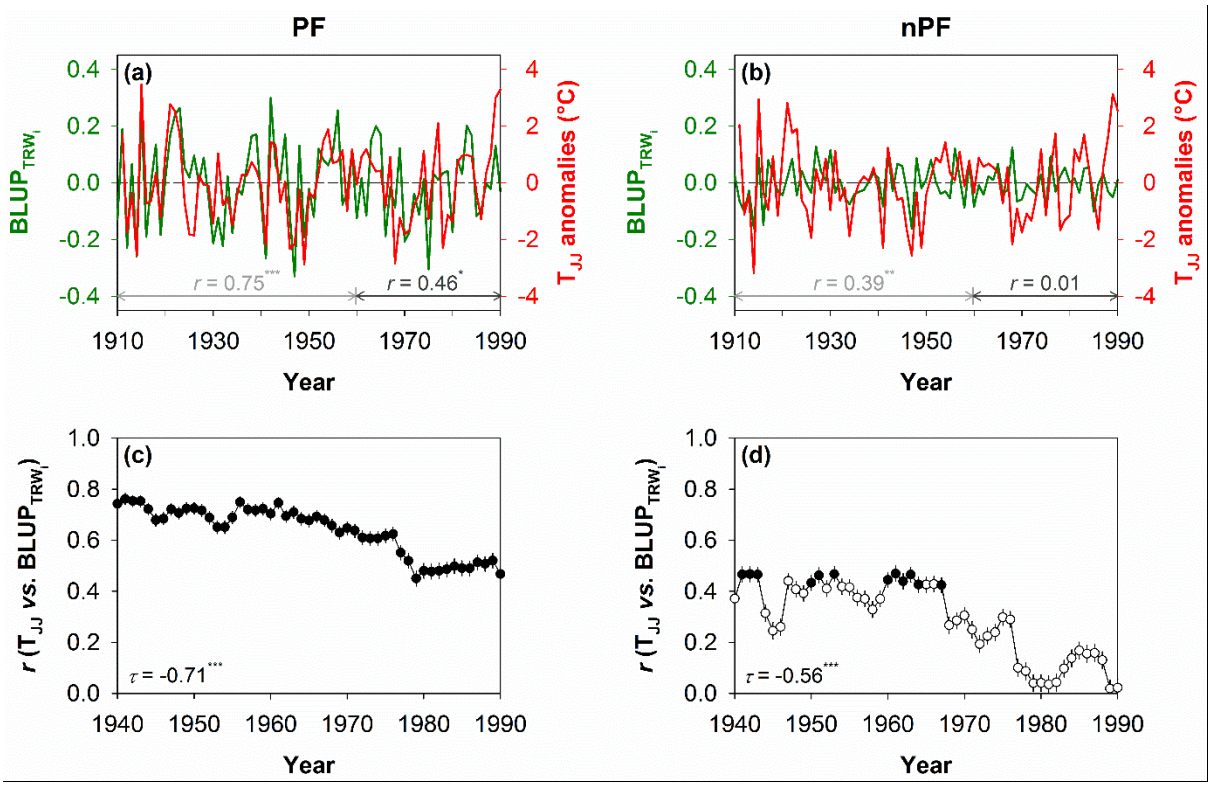


**Figure 5 (online colour only) (1.5 column fitting)**

**Figure 5.** Temporal variability in growth–climate relationships across landscape types for the period 1911–1990. (a,b) Aggregated (master) chronologies (green lines) and summer (June–July) temperature ($T_{JJ}$) anomalies (red lines) over time. The aggregated chronologies were derived as best linear unbiased predictors of tree-ring width indices ($BLUP_{TRWi}$) estimated from the best variance-covariance model for the study period (i.e., unstructured model) using a landscape classification as grouping criterion (i.e., permafrost [PF] or non-permafrost [nPF]). Correlations (*r*) between these two series are provided for the consecutive periods: 1911–1959 and 1960–1990. (c,d) Bootstrapped moving correlation analyses (*r*-values) between regional tree-ring width indices ($BLUP_{TRWi}$) and June–July temperature ($T_{JJ}$) for successive 30-year segments lagged by one year. Significant correlations are depicted as filled circles ($P < 0.05$). The standard errors of the estimates are shown as error bars. Years displayed on the *x*-axes correspond to the last year of 30-year moving intervals. Temporal

changes in growth–climate associations are characterised by Kendall's $\tau$. The asterisks after the $r$ ($\tau$) values indicate the level of significance: $^{**}P < 0.01$; $^{***}P < 0.001$.

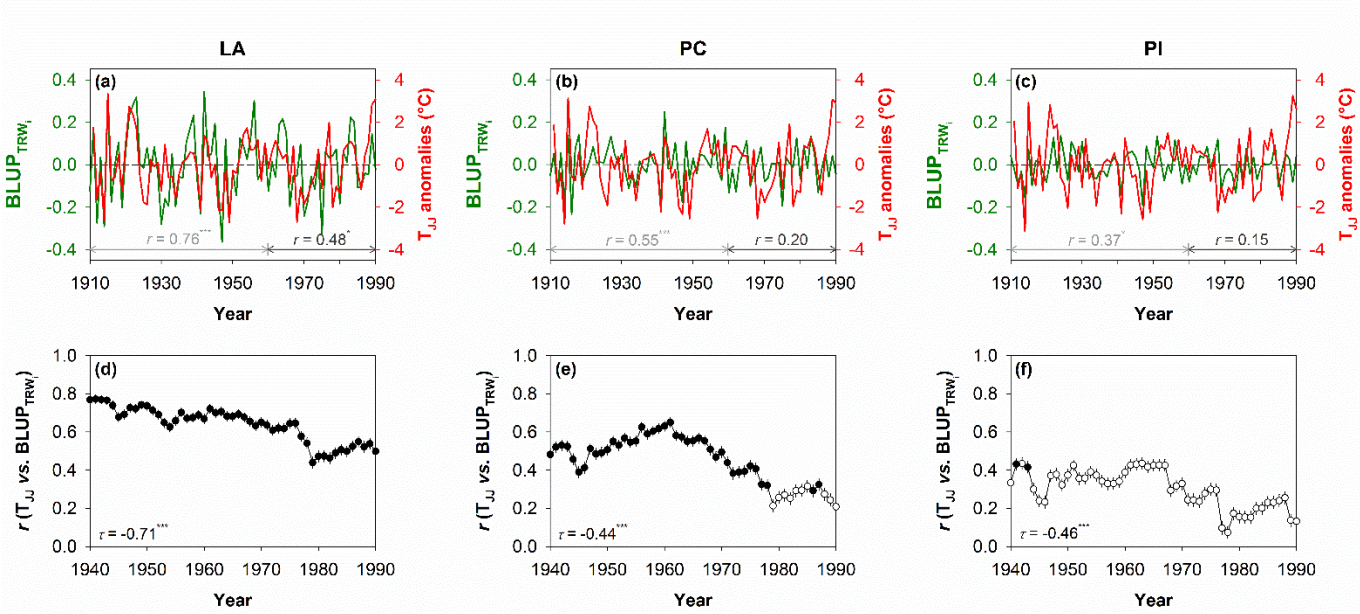


**Figure 6 (online colour only) (2 column fitting)**

**Figure 6.** Temporal variability in growth–climate relationships across genera for the period 1911–1990. (a,b,c) Aggregated (master) chronologies (green lines) and summer (June–July) temperature anomalies (red lines) over time. The aggregated chronologies were derived as best linear unbiased predictors of tree-ring indices ($BLUP_{TRWi}$) estimated from the best variance-covariance model for the study period (i.e., unstructured model) using a genus classification as grouping criterion (i.e., *Larix* [LA], *Picea* [PC] or *Pinus* [PI]). Correlations ($r$) between these two series are provided for the consecutive periods: 1911–1959 and 1960–1990. (d,e,f) Bootstrapped moving correlation analyses ($r$-values) between regional tree-ring indices ($BLUP_{TRWi}$) and June–July temperature ($T_{JJ}$) for successive 30-year segments lagged by one year. Significant correlations are depicted as filled circles ($P < 0.05$). The standard errors of the estimates are shown as error bars. Years displayed on the $x$-axes correspond to the last year of 30-year moving intervals. Temporal changes in growth–climate associations

586 are characterized by Kendall's $\tau$. The asterisks after the $r$ ($\tau$) values indicate the level of
587 significance: $^{*}P < 0.05$; $^{**}P < 0.01$; $^{***}P < 0.001$.
588
589
590 *3.7. Cointegration analysis*
591 The results of the unit root tests, *I(1)*, for $\hat{a}_{Ct}$ and $r_t$ are shown in Table A.3. Both
592 variables revealed non-stationarity at the landscape and genus level as indicated by
593 augmented Dickey-Fuller (ADF) tests. The variables became stationary after performing a
594 unit root test in the first difference (results not shown). This outcome led to evaluation of the
595 association between spatial synchrony and temperature-limited growth through a
596 cointegration test (Table 1). The results rejected the null hypothesis of no integration,
597 suggesting the presence of long-run equilibrium between $\hat{a}_{Ct}$ and $r_t$ that are *I(1)*, regardless of
598 landscape type and genus. The long-term trend of a relaxation of cold-limited growth on
599 synchrony is shown in Table 1. Overall, lower sensitive growth to summer temperature
600 reduced spatial synchrony, although PF showed non-significant long-run estimation for the
601 whole study period.
602 For nPF, the long-run effect was modest but significant (0.05-decrease in synchrony
603 for unit change in correlation between summer temperature and growth). For PF, the long-run
604 estimation reached significance after the break point in synchrony trend detected in 1959
605 ($b = 0.20$). At the genus level, significant or marginally significant long-run effects ranged
606 from 0.07 (*Pinus*) to 0.19 (*Picea*). K-M records extending until 2013 also showed a
607 significant long-run effect (Table 1).
608 The cointegration test also revealed that the short-run impacts ($\alpha_2$) of a relaxation of
609 cold-limited growth on synchrony were larger in magnitude than long-run effects (b) (Table
610 1). In addition, short-run effects were over fourfold larger in PF than in nPF. For example, a

(extreme) drop from 1 to 0 in growth-summer temperature relationship between two consecutive years would force synchrony to suddenly decrease by 0.31 (in PF) or 0.07 (in PF). Long- and short-run effects tended to equalize for PF after the 1959 break point in synchrony. Furthermore, the long-run effect exceeded that of short-run for the updated (post-1990) K-M records, reversing the $20^{th}$-century trend. At the genus level, short-run dynamics ranged from 0.16 (*Pinus*) to 0.32 (*Larix*), and long- and short-run effects were of about the same magnitude for *Picea*. Finally, the lagged correlation terms ($\alpha_3$) were negative and significant. This implied that after a disturbance decreasing cold-limited growth (i.e., a year having unusually high temperatures) and, hence, spatial synchrony, the synchrony variable reverted to equilibrium. For example, a coefficient of –0.096 for PF denoted that it would take about 10 years (1/0.096) for synchrony to return to pre-disturbance values following a strong decoupling between growth and temperature (or 10% of this disequilibrium is corrected in one year). In comparison, the period needed to return to equilibrium following decoupling was smaller in nPF (about 3 years), approximately constant across genera (4–5 years), and about 4 years for K-M.

**Table 1.** Output of the cointegration analysis for spatial synchrony ($\hat{a}_C$) and simple correlation ($r$) between aggregated tree-ring chronologies (BLUPs) at the landscape type or genus level and summer (June–July) temperature. Augmented Dickey-Fuller $\tau$ statistics (ADF test) are presented evaluating the null hypothesis of series unit root, *I(1)*, for residuals from the cointegrating regression models. Model parameters (see subsection 2.7) and goodness-of-fit ($r^2$) for error correction models (denoting short-term [annual] dynamics) and cointegrating regression models (denoting long-run [decadal] equilibrium) are shown. Changes in both variables ($\hat{a}_C$ and $r$) are characterized for successive 30-year segments lagged by one year for the period 1911–1990.

| | **Cointegration evaluation (ADF test)** | | **Error correction model (short–term dynamics)** | | | | **Cointegration regression model (long–term equilibrium)** | | |
|---|---|---|---|---|---|---|---|---|---|
| | $\tau$ | Prob. | $\alpha_2$ | $\alpha_3$ | $r^2$ | Prob. | b | $r^2$ | Prob. |
| *Landscape* | | | | | | | | | |
| PF | –2.23 | 0.026 | 0.312 [0.061] | –0.096 [0.064] | 0.405 | <0.001 | 0.018 [0.039] | 0.004 | 0.650 |
| $PF_{>1959}$[1] | –3.56 | <0.001 | 0.272 [0.078] | –0.109 [0.106] | 0.444 | <0.001 | 0.197 [0.028] | 0.623 | <0.001 |
| nPF | –2.67 | 0.009 | 0.069 [0.029] | –0.319 [0.110] | 0.246 | 0.001 | 0.048 [0.016] | 0.154 | 0.005 |
| *Genus* | | | | | | | | | |
| *Larix* | –2.88 | 0.005 | 0.321 [0.064] | –0.250 [0.093] | 0.417 | <0.001 | 0.127 [0.032] | 0.244 | <0.001 |
| *Picea* | –2.37 | 0.019 | 0.198 [0.077] | –0.203 [0.090] | 0.241 | 0.002 | 0.191 [0.039] | 0.328 | <0.001 |
| *Pinus* | –2.27 | 0.024 | 0.158 [0.043] | –0.213 [0.087] | 0.328 | <0.001 | 0.073 [0.040] | 0.063 | 0.075 |
| *Khanty-Mansiysk* | | | | | | | | | |
| K-M[2] | –2.62 | 0.009 | 0.032 [0.033] | –0.241[0.068] | 0.153 | 0.003 | 0.096 [0.021] | 0.219 | <0.001 |

[1] Calculated over the period 1960–1990

[2] Calculated over the period 1911–2013

## 4. Discussion

### *4.1. Regional tree-growth coherence and climate responses*

The temporal coherence in tree growth among stands differed considerably across boreal transcontinental Russia. Forests dwelling on permafrost showed a consistently greater (about two-fold) and geographically broader (up to 1,000 km) growth synchrony than non-permafrost forests. Furthermore, the extent of synchronous growth between non-permafrost forests declined exponentially, rather than linearly, up to inter-site distances of 500 km. Taxonomic differences in synchrony mimicked such a geographic pattern: the very cold-resistant *Larix sibirica* and, to a lesser extent, *Picea obovata* showed consistently higher synchrony compared with *Pinus* spp., mainly present at southern sites. Absence or presence of permafrost, rather than (mineral) soil type, is likely the main controlling factor differentiating ecosystem function in the area (Ping et al., 2015).

Enhanced temporal coherence among stands paralleled a northwards increase in sensitivity to summer temperature as a key driver of tree performance at the northern Russian timberline (Vaganov et al., 1999; Briffa et al., 2002; Wettstein et al., 2011; Hellmann et al., 2016; Tei and Sugimoto, 2018). Along a 800 km latitudinal gradient approaching 70°N, trees growing on permafrost were moderately to strongly limited by June–July temperatures, with substantially weaker temperature dependence of trees growing in the middle taiga (<65°N). Increasing cold limitation northwards was corroborated by a trend of decreasing tree-ring width in the region. Admittedly, the relevance of cold-temperature constrains for growth over permafrost was likely modulated by soil hydrothermal conditions (Körner and Hoch, 2006; Nikolaev et al., 2009). Intra-site growth coherence also increased northwards, differing markedly between permafrost and non-permafrost landscapes.

These spatial patterns suggest that increasingly complex combinations of abiotic factors and mechanistic drivers progressively influenced local tree growth below 65°N in the

transition zone between northern and middle taiga, hence decreasing spatial synchrony in tree-ring width signals. In particular, low or even absent responses to summer temperature were often accompanied by a positive reaction to summer precipitation, which is considered a typical indicator of water-stressed conifers, as reported for Eastern (Kagawa et al., 2003) or Central Siberia (Shestakova et al., 2017). Together with an extended vegetative period that is expected to result in miscellaneous growth responses to climate (Hellmann et al., 2016), a higher fire frequency in the middle taiga compared with northern zones (Sukhinin et al., 2004) also constitutes a probable contributor to the lower spatial synchrony observed among southern chronologies. Being intrinsically heterogeneous processes due to the spatial variability in fuel loads and topography, fires may cause populations to have asynchronous dynamics and, thus, reduce spatial agreement among them. Microsite variations and topography, as well as distance to water sources, are also prone to increasingly influencing tree growth responses southwards along the boreal biome (Düthorn et al., 2013; Kirdyanov et al., 2013; Linderholm et al., 2014). Disentangling soil and atmospheric effects on the carbon cycle is challenging (Ostle et al., 2009), and local factors are difficult to integrate when examining the interactions between physical and biological processes in boreal ecosystems and at broad scales as in this study (Esper et al., 2010).

Latitudinally structured growth–climate associations likely overlapped with species-specific differences in physiology and adaptive characteristics, including fire tolerance (Schulze et al., 2012). The most temperature-sensitive stands were dominated by larch and spruce, reflecting the natural distribution of forest types in the region (Tchebakova et al., 1994). In contrast, fir and pine forests, which demonstrate overall weak temperature limitation, are prevalent in the middle taiga (Blanchet et al., 2017).

*4.2. Widespread decreasing synchronous growth*

Decreasing trends in synchrony observed in permafrost (from 1960 onwards) and non-permafrost sites (across the 20$^{th}$ century) indicated more dissimilar growth patterns as climate warmed. The declining trend in synchrony was also evident across genera and spatial scales, including the smaller K-M area with records extending until 2013. Between-landscape and between-genera synchrony steadily decreased as well, although coherent growth patterns ($\hat{a}_C >> 0$) were still evident at the turn of this century. Altogether, these results suggest that tree performance in transcontinental Russia above 60°N is progressively being released from cold limitation as the fundamental driver of forest productivity in high-latitude ecosystems (Wettstein et al., 2011; St. George, 2014; Shestakova et al., 2018). Several lines of evidence point in this direction: first, a generalized weakening in site-level growth-climate associations after 1960; second, a robust temporal decline in the strength of growth–climate associations for the aggregated chronologies at the landscape and genus level; and finally, a decrease in short- and long-term dependences of synchrony on summer temperature over time as outlined by the cointegration analysis.

The two opening arguments point to a failure of ring-width records to follow high-frequency climate signals, a finding that is consistent with previous observations reporting divergence in year-to-year relationships between climate and tree rings in boreal forests (Briffa et al., 2002; D'Arrigo et al., 2009; Andreu-Hayles et al., 2011). As the climate warms, it is likely that non-synchronous endogenous disturbances (e.g., topography, nutrient availability, fire, permafrost melting and waterlogging, insect outbreaks) and species-specific imprints are acquiring relevance as factors controlling tree growth, reducing the effect of cold limitation regionally (Fajardo and McIntire, 2012; Ponocná et al., 2018). This warming-induced phenomenon was equally noticeable in permafrost and non-permafrost landscapes, although a complete loss of temperature sensitivity has gained recent strength at the

706 southernmost sites occupied by pine and spruce (below 65°N). Since our analysis focused on
707 high-frequency instability, the results were not affected by trend distortions that could
708 potentially occur if less flexible detrending methods had been applied (Melvin and Briffa,
709 2008). They are seemingly free of modern end standardization issues because the decrease in
710 temperature sensitivity is consistently observed for the period of 1960–1990 across spatial
711 domains (permafrost, non-permafrost) and for different temporal coverages, including
712 updated (post-1990) series. Our results are in contrast with recent trends of increasing growth
713 synchrony at other northern Eurasian regions (Briffa et al., 2008; Shestakova et al., 2016),
714 hence indicating changing drivers of tree performance across boreal Eurasia that deserve
715 careful examination. In this regard, the impact of boreal summer warming on growth patterns
716 seems to have counteracted an increasing geographic consistency of temperatures, which
717 instead could enhance synchrony (Fig. A.7). Interestingly, the lowest records of mean June–
718 July temperature that were registered during the 1940s are in agreement with a peak of
719 synchronous growth observed in permafrost sites in the mid-20$^{th}$ century, in agreement with
720 the principle of limiting factors (Hughes et al., 1982).

721 The post-1960 (BAI-derived) growth release observed at permafrost sites disagrees
722 with a potentially negative impact of increasing regional winter precipitation and consequent
723 delayed snowmelt on productivity (i.e., the shortening of the growing season; Vaganov et al.,
724 1999). A number of studies have shown a decrease in growth in boreal forests attributable to
725 temperature-induced moisture stress, as revealed by a shift from predominantly positive
726 correlations with temperature for the first half of the century to predominantly negative
727 correlations after 1950 (e.g., Briffa et al., 1998; D'Arrigo et al., 2004). We could not detect
728 such effect in our study sites. Instead, enhanced BAI in permafrost sites could be a
729 consequence of greater meristem activity owing to warmer summer temperatures (Körner,
730 2015). Another potential explanation relates to the well-known existence of adaptation lags in

the response of boreal conifers to their native conditions, in particular with regard to their temperature optima. Indeed, boreal trees exposed to warmer than native conditions show considerably faster growth rates, as documented in provenance trials (e.g., Rehfeldt et al., 2002; Way and Oren, 2010). Anyhow, the observed BAI changes would require confirmation by using more extensive records such as those derived from inventory-type data, which could also shed light on potential shifts in competitive balance between conifer species (Lloyd et al., 2011).

*4.3. Interpreting temperature effects on regional synchrony patterns*

Tests for cointegration between synchrony and *r*-values for temperature response indicated the presence of a long-run relationship between these variables. The long-run coefficients, however, suggested a varying dependence of growth synchrony on the magnitude of cold limitation between permafrost and non-permafrost sites. Reduced growth sensitivity to temperature gradually decreased 20$^{th}$-century coherence of tree growth across the permafrost-free middle taiga (including the K-M area). However, synchrony in the forest-tundra and northern taiga was negatively affected by a reduction of temperature response only after 1960, albeit at a *ca*. fourfold higher rate compared with the middle taiga. Although these effects were relatively modest, implying absolute decreases in spatial synchrony of *ca*. 0.1 in both landscapes, they were sufficiently relevant to be statistically sizable (considering that 20$^{th}$-century $\hat{a}_C$ was *ca*. 0.40 and 0.20 for permafrost and non-permafrost, respectively). At the northernmost sites, a weakening of temperature correlation decreasing spatial synchrony after 1960 suggests a temperature threshold for growth release from cold limitation of *ca*. 12°C in June–July (Moser et al., 2009). Temperatures exceeding critical thresholds enable an earlier and more intense cambial activity (e.g., Rossi et al., 2008), especially on trees growing on permafrost ground (Körner and Hoch, 2006), enhancing wood

formation but also exposing trees to other (local) factors influencing growth. These results reinforce the primary importance of June–July temperature variability in determining regional tree growth coherence in cold-limited ecosystems (Shestakova et al., 2016; Ponocná et al., 2018).

Conversely, synchrony did not adjust immediately to the equilibrium value implied by the long-run effect of temperature-limited growth. Instead, it is interesting to note that the short-run impacts of growth dependence on high temperatures in decreasing synchrony were generally larger than its long-run effects. This implies that in the short term the impact of a relaxation of cold-limited growth on synchrony was high, but this effect diminished with time. Tree species are able to cope with short-term disturbances (e.g., unusually high temperatures) through phenotypic plasticity and thus modulate long-term growth responses to environmental changes. Our results show that these short-term responses varied among species, with *Larix* being more responsive, followed by *Picea* and *Pinus*. This is in line with the relative degree of growth dependence on summer temperature of each species, which further corroborates how growth synchrony is predominantly driven by this climate factor across boreal transcontinental Russia. In contrast, we found a reverse trend for updated tree-ring records collected in the Khanty-Mansiysk area, with long-run impacts exceeding short-run effects. This suggests that, in spite of the fact that tree growth in the area is only weakly affected by temperature fluctuations, large-scale patterns of common growth variability are much influenced by recent warming trends. A similar effect is also anticipated by a large warming impact on permafrost sites observed after 1960. Finally, the lagged error correction terms indicated that the restitution period to revert to equilibrium was fairly uniform across genera, with about 20–25% of disequilibrium corrected per year (i.e., 4–5 years needed to return to equilibrium). Interestingly, large differences were observed between landscape types, with permafrost sites taking three times longer to recover from a high temperature

781 shock in comparison with permafrost-free stands. This finding reinforces the strong control of
782 permafrost on forest development through hydrological, thermal and biogeochemical
783 processes (Baltzer et al., 2014; Prokushkin et al., 2018). Our approach is complementary to
784 the analysis reported in D'Arrigo et al. (2004), in which cointegration techniques were
785 applied to demonstrate a statistically meaningful long-term relationship between ring-width
786 and summer temperatures. While the results of D'Arrigo et al. (2004) supported a recent shift
787 in the local response to temperature at elevational treeline in northwestern Canada, our study
788 reports on the underlying processes of synchrony changes in forest growth that are indicative
789 of a widespread contemporary impact of climate warming on boreal ecosystems.
790
791 *4.4. Conclusions*
792 Our results provide insights on the ways in which climate change impacts on boreal
793 forests can be traced back through the interpretation of synchrony patterns of tree-ring
794 networks. Unlike other studies in boreal (Briffa et al., 2008; Shestakova et al., 2016) and
795 temperate ecosystems (Black et al., 2017), we report a decreasing trend in spatial synchrony
796 of tree growth over the 20$^{th}$ century around the Ural Mountains. This phenomenon was
797 consistent across landscape types (permafrost and non-permafrost zones) and genera (*Larix*,
798 *Picea* and *Pinus*), and was accompanied by a positive warming effect on radial growth above
799 65°N. Importantly, our results reveal that changes in synchrony patterns were consistently
800 linked to growth release from cold limitation concurrent with regional climate warming. We
801 found that non-permafrost forest growth dynamics was progressively influenced by a loss of
802 temperature sensitivity over the 20$^{th}$ century. This process started in the 1960s in permafrost
803 sites, albeit at a rate several-fold higher, which resulted in comparable absolute decreases in
804 spatial synchrony among landscape types by the end of the 20$^{th}$ century. Other global factors
805 such as increasing atmospheric $CO_2$ concentration, global dimming, permafrost melting or N

deposition could have also played a role in the observed synchrony trends for the area. A thorough attribution analysis is complex and beyond the scope of this study, but their effect as drivers of synchrony may be comparatively scant in boreal ecosystems (Shestakova et al. 2016). Altogether, our findings contribute to unravel the spatiotemporal complexity of warming-induced relaxation of cold constrains on tree growth in boreal Eurasia, and demonstrate significant changes in forest dynamics of high-latitude ecosystems already taking place since the mid-20$^{th}$ century.

**Acknowledgments**

We thank P. Sopeña for technical assistance.

**Funding**

This study was funded by the European Union's Seventh Framework Programme (INTERACT project, grant agreement SYNCHROTREES), the Spanish Government (grant number AGL2015-68274-C3-3-R) and the Russian Science Foundation (project number 18-14-00072).

**Appendix A**

Appendix A contains supplementary data associated with this article.

## References


Agafonov, L.I., Gurskaya, M.A., 2013. The influence of the lower Ob River runoff on radial growth of trees. Contemporary Problems of Ecology 6(7), 779–787. https://doi.org/10.1134/s1995425513070159

Alday, J.G., Shestakova, T.A., Resco de Dios, V., Voltas, J., 2018. DendroSync: An R package to unravel synchrony patterns in tree-ring networks. Dendrochronologia 47, 17–22. https://doi.org/10.1016/j.dendro.2017.12.003

Allen, K.J., Villaba, R., Lavergne, A., Palmer, J.G., Cook, E.C., Fenwick, P., Drew, D.M., Turney, C.S.M., Baker, P.J., 2018. A comparison of some simple methods used to detect unstable temperature responses in tree-ring chronologies. Dendrochronologia 48, 52–73. https://doi.org/10.1016/j.dendro.2018.02.002

Anchukaitis, K.J., et al., 2017. Last millennium Northern Hemisphere summer temperatures from tree rings: Part II, spatially resolved reconstructions. Quaternary Science Reviews 163, 1–22. https://doi.org/10.1016/j.quascirev.2017.02.020

Andreu-Hayles, L., D'Arrigo, R., Anchukaitis, K.J., Beck, P.S.A., Frank, D., Goetz, S., 2011. Varying boreal forest response to Arctic environmental change at the Firth River, Alaska. Environmental Research Letters, 6(4), 045503. https://doi.org/10.1088/1748-9326/6/4/045503

Baltzer, J.L., Veness, T., Chasmer, L.E., Sniderhan, A.E., Quinton, W.L., 2014. Forests on thawing permafrost: Fragmentation, edge effects, and net forest loss. Global Change Biology 20(3), 824–834. https://doi.org/10.1111/gcb.12349

Biondi, F., Qeadan, F., 2008. A theory-driven approach to tree-ring standardization: Defining the biological trend from expected basal area increment. Tree-Ring Research 64(2), 81–96. https://doi.org/10.3959/2008-6.1

Black, B.A., et al., 2018. Rising synchrony controls western North American ecosystems. Global Change Biology 24(6), 2305–2314. https://doi.org/10.1111/gcb.14128

Blanchet, G., Guillet, S., Calliari, B., Corona, C., Edvardsson, J., Stoffel, M., Bragazza, L., 2017. Impacts of regional climatic fluctuations on radial growth of Siberian and Scots pine at Mukhrino mire (central-western Siberia). Science of the Total Environment 574, 1209–1216. https://doi.org/10.1016/j.scitotenv.2016.06.225

Briffa, K.R., Osborn, T.J., Schweingruber, F.H., Jones, P.D., Shiyatov, S.G., Vaganov, E.A., 2002. Tree-ring width and density data around the Northern Hemisphere: Part 1, local and regional climate signals. The Holocene 12(6), 737–757. https://doi.org/10.1191/0959683602hl587rp

Briffa, K.R., Schweingruber, F.H., Jones, P.D., Osborn, T.J., Shiyatov, S.G., Vaganov, E.A., 1998. Reduced sensitivity of recent tree-growth to temperature at high northern latitudes. Nature, 391(6668), 678–682. https://doi.org/10.1038/35596

Briffa, K.R., Shishov, V.V., Melvin, T.M., Vaganov, E.A., Grudd, H., Hantemirov, R. M., Eronen, M., Naurzbaev, M.M., 2008. Trends in recent temperature and radial tree growth spanning 2000 years across northwest Eurasia. Philosophical Transactions of the Royal Society B, 363(1501): 2271–2284. https://doi.org/10.1098/rstb.2007.2199

Brown, J., Ferrians, O., Heginbottom, J. A., Melnikov, E., 2002. Circum-Arctic map of permafrost and ground-ice conditions, Version 2. Boulder, Colorado USA. NSIDC: National Snow and Ice Data Center. [Accessed: 18 of June, 2018].

Brown, C.J., et al., 2011. Quantitative approaches in climate change ecology. Global Change Biology, 17(12), 3697–3713. https://doi.org/10.1111/j.1365-2486.2011.02531.x

Burnham, K.P., Anderson, D.R., 2002. Model selection and multimodel inference. (K. P. Burnham and D. R. Anderson, Eds.), *A practical information-theoretic approach* (488 pp). New York, NY: Springer Science and Business Media. https://doi.org/10.1007/b97636

874 Cook, E.R., Kairiukstis, L.A., 1990. Methods of dendrochronology: Applications in
875 the environmental sciences (394 pp). Dordrecht, The Netherlands*:* Kluwer Academic
876 Publishers.
877 Cook, E.R., Krusic, P.J., 2005. Program ARSTAN: A tree-ring standardization
878 program based on detrending and autoregressive time series modeling, with interactive
879 graphics. Lamont-Doherty Earth Observatory, Columbia University, Palisades, NY.
880 D'Arrigo, R., Jacoby, G., Buckley, B., Sakulich, J., Frank, D., Wilson, R., Curtis, A.,
881 Anchukaitis, K., 2009. Tree growth and inferred temperature variability at the North
882 American Arctic treeline. Global and Planetary Change 65(1–2), 71–82.
883 https://doi.org/10.1016/j.gloplacha.2008.10.011
884 D'Arrigo, R., Kaufmann, R.K., Davi, N., Jacoby, G.C., Laskowski, C., Myneni, R.B.,
885 Cherubini, P., 2004. Thresholds for warming-induced growth decline at elevational tree line
886 in the Yukon Territory, Canada. Global Biogeochemical Cycles 18(3), GB3021.
887 https://doi.org/10.1029/2004GB002249
888 Düthorn, E., Holzkämper, S., Timonen, M., Esper, J. 2013. Influence of micro-site
889 conditions on tree-ring climate signals and trends in central and northern Sweden. Trees -
890 Structure and Function 27(5), 1395–1404. https://doi.org/10.1007/s00468-013-0887-8
891 Engle, R.F., Granger, C.W.J., 1987. Co-integration and error correction:
892 Representation, estimation, and testing. Econometrica 55(2), 251–276.
893 https://doi.org/10.2307/1913236
894 Esper, J., Frank, D., Büntgen, U., Verstege, A., Hantemirov, R., Kirdyanov, A. V.,
895 2010. Trends and uncertainties in Siberian indicators of 20th century warming. Global
896 Change Biology 16(1), 386–398. https://doi.org/10.1111/j.1365-2486.2009.01913.x

Fajardo, A., McIntire, E.J.B., 2012. Reversal of multicentury tree growth improvements and loss of synchrony at mountain tree lines point to changes in key drivers. Journal of Ecology 100(3), 782–794. https://doi.org/10.1111/j.1365-2745.2012.01955.x

Fortin, M.J., Gurevitch, J., 1993. Mantel tests: Spatial structure in field experiments. (S. Scheiner and J. Gurevitch, Eds.), *Design and analysis of ecological experiments* (445 pp). New York, NY: Chapman & Hall.

Friedman, J.H. 1984. A variable span smoother. Technical Report No. 5. Stanford University.

Girardin, M.P., Bouriaud, O., Hogg, E.H., Kurz, W., Zimmermann, N.E., Metsaranta, J.M., de Jong, R., Frank, D.C., Esper, J., Büntgen, U., Guo, X.J., Bhatti, J., 2016. No growth stimulation of Canada's boreal forest under half-century of combined warming and $CO_2$ fertilization. Proceedings of the National Academy of Sciences 113(52), E8406–E8414. doi:10.1073/pnas.1610156113

Grissino-Mayer, H.D., Fritts, H.C., 1997. The international tree-ring data bank: An enhanced global database serving the global scientific community. Holocene 7(2), 235–238. https://doi.org/10.1177/095968369700700212

Harris, I., Jones, P.D., Osborn, T.J., Lister, D.H., 2014. Updated high-resolution grids of monthly climatic observations - the CRU TS3.10 Dataset. International Journal of Climatology 34(3), 623–642. https://doi.org/10.1002/joc.3711

Hellmann, L., et al., 2016. Diverse growth trends and climate responses across Eurasia's boreal forest. Environmental Research Letters 11, Art. 074021. https://doi.org/10.1088/1748-9326/11/7/074021

Holmes, R.L., 1983. Computer-assisted quality control in tree-ring dating and measurement. Tree-Ring Bulletin 43, 69–78. https://doi.org/10.1016/j.ecoleng.2008.01.004

Hughes, M.K., Kelly, P.M., Pilcher, J.R., La Marche, V.C. Jr., 1982. Climate from tree rings. Cambridge University Press, Cambridge.

Jacoby, G.C., D'Arrigo, R.D., 1995. Tree ring width and density evidence of climatic and potential forest change in Alaska. Global Biogeochemical Cycles 9(2), 227–234. https://doi.org/10.1029/95GB00321

Jacoby, G.C., Lovelius, N.V., Shumilov, O.I., Raspopov, O.M., Karbainov, J.M., Frank, D.C., 2000. Long-term temperature trends and tree growth in the Taymir region of northern Siberia. Quaternary Research 53(3), 312–318. https://doi.org/10.1006/qres.2000.2130

Kagawa, A., Naito, D., Sugimoto, A., Maximov, T.C., 2003. Effects of spatial and temporal variability in soil moisture on widths and $\delta^{13}C$ values of eastern Siberian tree rings. Journal of Geophysical Research 108(D16), 4500. https://doi.org/10.1029/2002JD003019

Kirchgässner, G., Wolters, J., 2007. Introduction to modern time series analysis. Springer Berlin Heidelberg.

Kirdyanov, A., Hughes, M., Vaganov, E., Schweingruber, F., Silkin, P., 2003. The importance of early summer temperature and date of snow melt for tree growth in the Siberian Subarctic. Trees - Structure and Function 17(1), 61–69. https://doi.org/10.1007/s00468-002-0209-z

Kirdyanov, A. V., Prokushkin, A. S., Tabakova, M. A., 2013. Tree-ring growth of Gmelin larch under contrasting local conditions in the north of Central Siberia. Dendrochronologia 31(2), 114–119. https://doi.org/10.1016/j.dendro.2012.10.003

Kirpotin, S.N., et al., 2009. Western Siberia wetlands as indicator and regulator of climate change on the global scale. International Journal of Environmental Studies 66(4), 409–421. https://doi.org/10.1080/00207230902753056

945 Knorre, A.A., Kirdyanov, A.V., Vaganov, E.A., 2006. Climatically induced
946 interannual variability in aboveground production in forest-tundra and northern taiga of
947 central Siberia. Oecologia 147(1), 86–95. https://doi.org/10.1007/s00442-005-0248-4
948 Koenig, W.D., Knops, J.M.H., 1998. Testing for spatial autocorrelation in ecological
949 studies. Ecography 21(4), 423–429. https://doi.org/10.1111/j.1600-0587.1998.tb00407.x
950 Körner, C., 2015. Paradigm shift in plant growth control. Current Opinion in Plant
951 Biology 25, 107–114. https://doi.org/10.1016/j.pbi.2015.05.003
952 Körner, C., Hoch, G., 2006. A test of treeline theory on a montane permafrost island.
953 Arctic, Antarctic, and Alpine Research 38(1), 113–119. https://doi.org/10.1657/1523-
954 0430(2006)038[0113:ATOTTO]2.0.CO;2
955 Linderholm, H.W., et al., 2014. Growth dynamics of tree-line and lake-shore Scots
956 pine (*Pinus sylvestris* L.) in the central Scandinavian Mountains during the Medieval Climate
957 Anomaly and the early Little Ice Age. Frontiers in Ecology and Evolution 2, 20.
958 https://doi.org/10.3389/fevo.2014.00020
959 Lloyd, A.H., Bunn, A.G., Berner, L., 2011. A latitudinal gradient in tree growth
960 response to climate warming in the Siberian taiga. Global Change Biology 17(5), 1935–1945.
961 https://doi.org/10.1111/j.1365-2486.2010.02360.x
962 Melvin, T.M., Briffa, K.R., 2008. A "signal-free" approach to dendroclimatic
963 standardisation. Dendrochronologia 26(2), 71–86.
964 https://doi.org/10.1016/j.dendro.2007.12.001
965 Moser, L., Fonti, P., Büntgen, U., Esper, J., Luterbacher, J., Franzen, J., Frank, D.,
966 2009. Timing and duration of European larch growing season along altitudinal gradients in
967 the Swiss Alps. Tree Physiology 30(2), 225–233. https://doi.org/10.1093/treephys/tpp108

968 Murray, M. P., 1994. A drunk and her dog: an illustration of cointegration and error
969 correction. The American Statistician 48(1), 37–39.
970 https://doi.org/10.1080/00031305.1994.10476017
971 Nikolaev, A.N., Fedorov, P.P., Desyatkin, A. R., 2009. Influence of climate and soil
972 hydrothermal regime on radial growth of *Larix cajanderi* and *Pinus sylvestris* in central
973 Yakutia, Russia. Scandinavian Journal of Forest Research 24(3), 217–226.
974 https://doi.org/10.1080/02827580902971181
975 Ols, C., Girardin, M.P., Hofgaard, A., Bergeron, Y., Drobyshev, I., 2018a. Monitoring
976 climate sensitivity shifts in tree-rings of Eastern Boreal North America using model-data
977 comparison: shifts in tree growth sensitivity to climate. Ecosystems 21(5), 1042–1057.
978 https://doi.org/10.1007/s10021-017-0203-3
979 Ols, C., Trouet, V., Girardin, M.P., Hofgaard, A., Bergeron, Y., Drobyshev, I., 2018b.
980 Post-1980 shifts in the sensitivity of boreal tree growth to North Atlantic Ocean dynamics
981 and seasonal climate. Global and Planetary Change 165, 1–12.
982 https://doi.org/10.1016/j.gloplacha.2018.03.006
983 Ostle, N.J., et al., 2009. Integrating plant-soil interactions into global carbon cycle
984 models. Journal of Ecology 97(5), 851–863. https://doi.org/10.1111/j.1365-
985 2745.2009.01547.x
986 Ping, C.L., Jastrow, J.D., Jorgenson, M.T., Michaelson, M.T., Shur, Y.L., 2015.
987 Permafrost soils and carbon cycling. Soil 1, 147–171. https://doi.org/10.5194/soil-1-147-2015
988 Ponocná, T., Chuman, T., Rydval, M., Urban, G., Migała, K., Treml, V., 2018.
989 Deviations of treeline Norway spruce radial growth from summer temperatures in East-
990 Central Europe. Agricultural and Forest Meteorology 253–254, 62–70.
991 https://doi.org/10.1016/j.agrformet.2018.02.001

992 Prokushkin, A.S., Hagedorn, F., Pokrovsky, O.S., Viers, J., Kirdyanov, A.V.,
993 Masyagina, O.V., Prokushkina, M.P., McDowell, W.H., 2018. Permafrost regime affects the
994 nutritional status and productivity of larches in Central Siberia. Forests 9(6), 314.
995 https://doi.org/10.3390/f9060314
996 Rehfeldt, G.E., Tchebakova, N.M., Parfenova, Y.I., Wykoff, W.R., Kuzmina, N.A.,
997 Milyutin, L.I. (2002). Intraspecific responses to climate in *Pinus sylvestris*. Global Change
998 Biology 8(9), 912–919. https://doi.org/10.1046/j.1365-2486.2002.00516.x
999 Rossi, S., Deslauriers, A., Griçar, J., Seo, J.W., Rathgeber, C.B.K., Anfodillo, T.,
1000 Morin, H., Levanic, T., Oven, P., Jalkanen, R., 2008. Critical temperatures for xylogenesis in
1001 conifers of cold climates. Global Ecology and Biogeography 17(6), 696–707.
1002 https://doi.org/10.1111/j.1466-8238.2008.00417.x
1003 Sedykh, V.N., 1996. The forests of western Siberia and the oil and gas complex.
1004 Ekologia (in Russian). Moscow.
1005 Shestakova, T.A., Aguilera, M., Ferrio, J.P., Gutiérrez, E., Voltas, J., 2014.
1006 Unravelling spatiotemporal tree-ring signals in Mediterranean oaks: A variance-covariance
1007 modelling approach of carbon and oxygen isotope ratios. Tree Physiology 34(8), 819–838.
1008 https://doi.org/10.1093/treephys/tpu037
1009 Shestakova, T.A., Gutiérrez, E., Kirdyanov, A.V., Camarero, J.J., Génova, M.,
1010 Knorre, A.A., Linares, J.C., Resco de Dios, V., Sánchez-Salguero, R., Voltas, J., 2016.
1011 Forests synchronize their growth in contrasting Eurasian regions in response to climate
1012 warming. Proceedings of the National Academy of Sciences 113(3), 662–667.
1013 https://doi.org/10.1073/pnas.1514717113
1014 Shestakova, T.A., Gutiérrez, E., Voltas, J., 2018. A roadmap to disentangling
1015 ecogeographical patterns of spatial synchrony in dendrosciences. Trees - Structure and
1016 Function 32(2), 359–370. https://doi.org/10.1007/s00468-017-1653-0

Shestakova, T.A., Voltas, J., Saurer, M., Siegwolf, R.T.W., Kirdyanov, A.V., 2017. Warming effects on *Pinus sylvestris* in the cold-dry Siberian forest-steppe: Positive or negative balance of trade? Forests 8(12), 490. https://doi.org/10.3390/f8120490

Schulze, E.D., Wirth, C., Mollicone, D., Von Lüpke, N., Ziegler, W., Achard, F., Mund, M., Prokushkin, A., Scherbina, S., 2012. Factors promoting larch dominance in central Siberia: Fire versus growth performance and implications for carbon dynamics at the boundary of evergreen and deciduous conifers. Biogeosciences 9(4), 1405–1421. https://doi.org/10.5194/bg-9-1405-2012

St. George, S., 2014. An overview of tree-ring width records across the Northern Hemisphere. Quaternary Science Reviews 95, 132–150. https://doi.org/10.1016/j.quascirev.2014.04.029

Sukhinin, A.I., et al., 2004. AVHRR-based mapping of fires in Russia: New products for fire management and carbon cycle studies. Remote Sensing of Environment 93(4), 546–564. https://doi.org/10.1016/j.rse.2004.08.011

Tchebakova, N.M., Monserud, R.A., Nazimova, D.I., 1994. A Siberian vegetation model-based on climatic parameters. Canadian Journal of Forest Research 24(8), 1597–1607. https://doi.org/10.1139/x94-208

Tei, S., Sugimoto, A., 2018. Time lag and negative responses of forest greenness and tree growth to warming over circumboreal forests. Global Change Biology. https://doi.org/10.1111/gcb.14135

Trouet, V., Panayotov, M.P., Ivanova, A., Frank, D., 2012. A pan-European summer teleconnection mode recorded by a new temperature reconstruction from the northeastern Mediterranean (AD 1768–2008). Holocene 22(8), 887–898. https://doi.org/10.1177/0959683611434225

Vaganov, E.A., Hughes, M.K., Kirdyanov, A.V., Schweingruber, F.H., Silkin, P.P., 1999. Influence of snowfall and melt timing on tree growth in subarctic Eurasia. Nature 400(6740), 149–151. https://doi.org/10.1038/22087

Way, D.A., Oren, R., 2010. Differential responses to changes in growth temperature between trees from different functional groups and biomes: a review and synthesis of data. Tree Physiology 30(6), 669–688. https://doi:10.1093/treephys/tpq015

Wettstein, J.J., Littell, J.S., Wallace, J.M., Gedalof, Z., 2011. Coherent region-, species-, and frequency-dependent local climate signals in Northern hemisphere tree-ring widths. Journal of Climate 24(23), 5998–6012. https://doi.org/10.1175/2011JCLI3822.1

Wigley, T.M.L., Briffa, K.R., Jones, P.D., 1984. On the average value of correlated time series, with applications in dendroclimatology and hydrometeorology. Journal of Climate and Applied Meteorology 23(2), 201–213. https://doi.org/10.1175/1520-0450(1984)023<0201:OTAVOC>2.0.CO;2

Zang, C., Biondi, F., 2015. Treeclim: An R package for the numerical calibration of proxy-climate relationships. Ecography 38(4), 431–436. https://doi.org/10.1111/ecog.01335

Zeileis, A., Leisch, F., Hornik, K., Kleiber, C., 2002. strucchange: An R package for testing for structural change in linear regression models. Journal of Statistical Software 7(2), 1–38. https://doi.org/10.18637/jss.v007.i02

# Appendix A

**Table A.1.** Geographical, climatic and dendrochronological characteristics of the sampling sites. For tree-ring chronologies derived from the International Tree-Ring Data Bank (ITRDB), the corresponding reference code is provided. Abbreviations: MAT, mean annual temperature; MST, mean summer (June–August) temperature; MAP, mean annual precipitation; MSP, mean summer (June–August) precipitation; MWP, mean winter (December–February) precipitation; *EPS*, Expressed Population Signal; *Rbar*, mean interseries correlation, TRW, tree-ring width. Mean climatic values and chronology statistics are calculated over the period 1911–1990. The variability of mean TRW values is expressed as standard deviation (SD).

| Site | Code | ITRDB reference | Latitude (°N) | Longitude (°E) | Altitude (m a.s.l.) | MAT (°C) | MST (°C) | MAP (mm) | MSP (mm) | MWP (mm) | Nr trees (cores) | Time span | Median (min/max) age (years) | *EPS* > 0.85 | *Rbar* | Mean TRW ± SD (mm) |
|---|---|---|---|---|---|---|---|---|---|---|---|---|---|---|---|---|
| *Larix sibirica* (LASI) | | | | | | | | | | | | | | | | |
| 1 | LASI1 | russ223 | 67°30' | 70°00' | 30 | –7.6 | 9.2 | 369 | 140 | 60 | 50(50) | 1580–2000 | 159 (102/415) | 1710 | 0.61 | 0.74±0.27 |
| 2 | LASI2 | russ092 | 67°28' | 76°46' | 20 | –8.5 | 9.3 | 430 | 150 | 79 | 14(27) | 1585–1990 | 279 (66/406) | 1710 | 0.66 | 0.33±0.14 |
| 3 | LASI3 | russ035 | 67°12' | 69°49' | 90 | –7.3 | 9.6 | 384 | 147 | 63 | 12(23) | 1782–1990 | 81 (66/196) | 1816 | 0.58 | 0.56±0.27 |
| 4 | LASI4 | russ220 | 66°54' | 65°35' | no data | –10.4 | 6.5 | 541 | 217 | 77 | 34(57) | 1637–1990 | 171 (67/354) | 1710 | 0.42 | 0.56±0.07 |
| 5 | LASI5 | russ021 | 66°52' | 65°37' | 250 | –8.9 | 8.1 | 505 | 201 | 73 | 16(27) | 1637–1990 | 158 (97/354) | 1710 | 0.66 | 0.39±0.14 |
| 6 | LASI6 | russ224 | 66°49' | 65°34' | 190 | –6.9 | 10.3 | 454 | 179 | 67 | 18(28) | 1641–2001 | 293 (75/360) | 1710 | 0.70 | 0.42±0.17 |
| 7 | LASI7 | russ225 | 66°49' | 65°34' | 190 | –6.9 | 10.3 | 454 | 179 | 67 | 17(24) | 1845–2006 | 114 (85/162) | 1887 | 0.70 | 0.86±0.38 |
| 8 | LASI8 | russ064 | 66°13' | 56°19' | 65 | –3.1 | 12.1 | 506 | 167 | 97 | 13(26) | 1630–1990 | 201 (97/361) | 1710 | 0.61 | 0.43±0.12 |
| 9 | LASI9 | russ101 | 66°13' | 71°40' | 80 | –7.4 | 9.8 | 427 | 159 | 72 | 17(34) | 1740–1990 | 146 (83/251) | 1829 | 0.52 | 0.37±0.19 |
| 10 | LASI10 | russ122 | 66°04' | 77°40' | 50 | –4.4 | 11.3 | 725 | 282 | 114 | 13(26) | 1780–1990 | 135 (64/211) | 1816 | 0.60 | 0.50±0.19 |

| Site | Code | ITRDB reference | Latitude (°N) | Longitude (°E) | Altitude (m a.s.l.) | MAT (°C) | MST (°C) | MAP (mm) | MSP (mm) | MWP (mm) | Nr trees (cores) | Time span | Median (min/max) age (years) | *EPS* > 0.85 | *Rbar* | Mean TRW ± SD (mm) |
|---|---|---|---|---|---|---|---|---|---|---|---|---|---|---|---|---|
| 11 | LASI11 | russ082 | 66°04' | 77°40' | 30 | –3.1 | 12.1 | 506 | 167 | 97 | 14(27) | 1671–1990 | 139 (102/320) | 1791 | 0.55 | 0.64±0.20 |
| 12 | LASI12 | russ123 | 65°27' | 60°34' | 400 | –5.5 | 10.4 | 545 | 194 | 90 | 10(20) | 1588–1990 | 337 (221/403) | 1710 | 0.76 | 0.19±0.07 |
| 13 | LASI13 | russ084 | 65°22' | 72°52' | 100 | –6.5 | 11 | 452 | 168 | 76 | 15(29) | 1767–1990 | 190 (96/224) | 1796 | 0.51 | 0.68±0.28 |
| 14 | LASI14 | russ180 | 65°19' | 64°39' | 30 | –4.6 | 12.6 | 487 | 188 | 73 | 13(26) | 1828–1994 | 137 (105/167) | 1856 | 0.67 | 0.99±0.43 |
| 15 | LASI15 | russ159 | 63°04' | 76°19' | 170 | –4.9 | 13.4 | 536 | 212 | 81 | 12(24) | 1804–1994 | 165 (133/191) | 1836 | 0.62 | 0.47±0.20 |
| 16 | LASI16 | K-M | 61°29' | 66°03' | 77 | –1.5 | 15.3 | 563 | 224 | 83 | 15(26) | 1871–2013 | 103 (69/144) | 1903 | 0.42 | 1.10±0.45 |
| 17 | LASI17 | russ117 | 60°22' | 57°07' | 140 | 0.6 | 15.6 | 690 | 232 | 134 | 14(28) | 1730–1991 | 194 (133/262) | 1782 | 0.50 | 0.87±0.36 |
| *Picea obovata* (PCOB) | | | | | | | | | | | | | | | | |
| 1 | PCOB1 | russ237 | 67°49' | 60°01' | 75 | –5.9 | 9.5 | 419 | 143 | 74 | 15(29) | 1751–2000 | 161 (95/250) | 1810 | 0.54 | 0.51±0.19 |
| 2 | PCOB2 | russ022 | 66°52' | 65°37' | 250 | –8.9 | 8.1 | 505 | 201 | 73 | 18(32) | 1663–1990 | 199 (67/328) | 1761 | 0.34 | 0.34±0.08 |
| 3 | PCOB3 | russ034 | 66°49' | 69°16' | 90 | –6.8 | 10.2 | 400 | 156 | 63 | 12(24) | 1710–1990 | 195 (83/268) | 1778 | 0.45 | 0.33±0.09 |
| 4 | PCOB4 | russ042 | 66°13' | 56°19' | 65 | –3.1 | 12.1 | 506 | 167 | 97 | 12(24) | 1784–1990 | 197 (151/207) | 1816 | 0.35 | 0.51±0.14 |
| 5 | PCOB5 | russ032 | 66°07' | 71°40' | 80 | –7.2 | 10 | 429 | 160 | 72 | 12(24) | 1720–1990 | 131 (55/271) | 1763 | 0.54 | 0.47±0.15 |
| 6 | PCOB6 | russ033 | 66°04' | 77°40' | 30 | –7.3 | 11.3 | 478 | 171 | 83 | 13(26) | 1752–1990 | 161 (81/234) | 1811 | 0.51 | 0.61±0.15 |
| 7 | PCOB7 | russ037 | 65°30' | 72°39' | 100 | –6.6 | 10.9 | 451 | 167 | 76 | 15(30) | 1794–1990 | 178 (60/197) | 1826 | 0.42 | 0.54±0.13 |
| 8 | PCOB8 | russ097 | 65°20' | 69°31' | 25 | –5.6 | 11.9 | 462 | 181 | 73 | 18(34) | 1601–1991 | 172 (84/391) | 1710 | 0.44 | 0.62±0.10 |
| 9 | PCOB9 | russ177 | 63°07' | 75°19' | 150 | –5.1 | 13.1 | 544 | 214 | 83 | 13(26) | 1855–1994 | 116 (47/145) | 1890 | 0.41 | 1.30±0.35 |
| 10 | PCOB10 | russ095 | 62°36' | 58°47' | 340 | –3.2 | 12.6 | 679 | 247 | 117 | 15(29) | 1616–1991 | 205 (126/376) | 1787 | 0.50 | 0.78±0.24 |
| 11 | PCOB11 | russ120 | 61°16' | 59°19' | 670 | –4.4 | 11.3 | 725 | 282 | 114 | 14(28) | 1703–1993 | 218 (111/291) | 1808 | 0.47 | 0.35±0.13 |
| 12 | PCOB12 | K-M | 61°00' | 69°02' | 69 | –1.6 | 15.6 | 550 | 220 | 80 | 10(15) | 1858–2013 | 139 (65/157) | 1909 | 0.41 | 1.42±0.47 |
| 13 | PCOB13 | K-M | 60°54' | 68°42' | 33 | –1.1 | 15.9 | 540 | 216 | 78 | 15(24) | 1841–2013 | 118 (59/174) | 1873 | 0.44 | 1.65±0.70 |
| 14 | PCOB14 | russ104 | 60°22' | 57°07' | 140 | 0.6 | 15.6 | 690 | 232 | 134 | 16(32) | 1680–1991 | 211 (118/312) | 1750 | 0.40 | 0.73±0.20 |
| 15 | PCOB15 | K-M | 60°05' | 69°27' | 32 | –0.9 | 15.9 | 524 | 215 | 74 | 14(22) | 1854–2013 | 105 (85/161) | 1888 | 0.35 | 2.32±0.90 |
| *Pinus sylvestris* (PISY) | | | | | | | | | | | | | | | | |
| 1 | PISY1 | russ046 | 66°13' | 56°19' | 65 | –3.1 | 12.1 | 506 | 167 | 97 | 14(24) | 1694–1990 | 207 (153/297) | 1726 | 0.45 | 0.46±0.16 |
| 2 | PISY2 | russ100 | 65°17' | 69°40' | 35 | –5.6 | 11.7 | 464 | 181 | 73 | 13(26) | 1674–1991 | 161 (78/317) | 1710 | 0.39 | 0.56±0.22 |
| 3 | PISY3 | russ244 | 63°32' | 69°10' | 63 | –3.9 | 13.5 | 530 | 208 | 81 | 30(30) | 1588–2006 | 341 (192/415) | 1710 | 0.33 | 0.41±0.08 |
| 4 | PISY4 | russ155 | 62°55' | 76°22' | 180 | –4.8 | 13.6 | 536 | 213 | 81 | 13(26) | 1726–1994 | 185 (146/269) | 1796 | 0.52 | 0.46±0.10 |

| Site | Code | ITRDB reference | Latitude (°N) | Longitude (°E) | Altitude (m a.s.l.) | MAT (°C) | MST (°C) | MAP (mm) | MSP (mm) | MWP (mm) | Nr trees (cores) | Time span | Median (min/max) age (years) | *EPS* > 0.85 | *Rbar* | Mean TRW ± SD (mm) |
|---|---|---|---|---|---|---|---|---|---|---|---|---|---|---|---|---|
| 5 | PISY5 | K-M | 61°29' | 66°03' | 77 | –1.5 | 15.3 | 563 | 224 | 83 | 15(21) | 1900–2013 | 75 (61/115) | 1922 | 0.43 | 2.06±0.60 |
| 6 | PISY6 | K-M | 61°05' | 69°29' | 35 | –1.6 | 15.5 | 543 | 218 | 79 | 14(21) | 1910–2013 | 94 (75/105) | 1921 | 0.35 | 1.98±1.05 |
| 7 | PISY7 | K-M | 60°59' | 69°01' | 67 | –1.3 | 15.8 | 544 | 217 | 79 | 15(23) | 1931–2013 | 66 (55/84) | 1945 | 0.33 | 2.60±1.37 |
| 8 | PISY8 | russ099 | 60°34' | 59°32' | 720 | –1.0 | 14.4 | 590 | 244 | 84 | 13(26) | 1612–1992 | 137 (90/378) | 1710 | 0.45 | 0.81±0.24 |
| 9 | PISY9 | K-M | 60°32' | 68°25' | 38 | –0.9 | 15.9 | 535 | 216 | 76 | 20(36) | 1827–2013 | 111 (70/188) | 1858 | 0.40 | 1.37±0.44 |
| 10 | PISY10 | russ116 | 60°22' | 57°07' | 140 | 0.6 | 15.6 | 690 | 232 | 134 | 15(30) | 1717–1991 | 160 (103/275) | 1838 | 0.36 | 0.92±0.23 |
| *Pinus sibirica* (PISI) | | | | | | | | | | | | | | | | |
| 1 | PISI1 | K-M | 60°59' | 69°01' | 67 | –1.3 | 15.8 | 544 | 217 | 79 | 10(16) | 1788–2013 | 145 (72/227) | 1855 | 0.39 | 2.01±0.82 |
| 2 | PISI2 | K-M | 60°32' | 68°25' | 38 | –0.9 | 15.9 | 535 | 216 | 76 | 15(24) | 1852–2013 | 99 (78/163) | 1893 | 0.35 | 1.80±0.36 |
| 3 | PISI2 | K-M | 60°05' | 69°27' | 32 | –0.9 | 15.9 | 524 | 215 | 74 | 15(23) | 1855–2013 | 124 (53/160) | 1870 | 0.38 | 2.03±0.41 |
| *Abies sibirica* (ABSI) | | | | | | | | | | | | | | | | |
| 1 | ABSI1 | K-M | 61°00' | 69°02' | 69 | –1.6 | 15.6 | 550 | 220 | 80 | 12(16) | 1870–2013 | 110 (75/145) | 1893 | 0.33 | 1.54±0.41 |
| 2 | ABSI2 | K-M | 60°54' | 68°42' | 33 | –1.1 | 15.9 | 540 | 216 | 78 | 13(19) | 1857–2013 | 102 (74/158) | 1904 | 0.32 | 1.31±0.37 |
| 3 | ABSI3 | K-M | 60°05' | 69°27' | 32 | –0.9 | 15.9 | 524 | 215 | 74 | 10(13) | 1916–2013 | 79 (71/99) | 1941 | 0.28 | 2.49±0.66 |

10

**Table A.2.** Long-term changes in radial growth for old trees (>200 years) across landscape types and genera. Growth rates (assessed as basal area increment, BAI) for each site–genus combination were subjected to a linear mixed-effects model. The values are given as mean ± SE ($cm^2$ $year^{-1}$) and *n* stands for the number of chronologies used. For each tree class, mean values in a row followed by the same letter are not significantly different based on Student's *t*-test ($P < 0.05$). BAI values were log-transformed for analysis.

| Group | 1911–1959 | 1960–1990 | *n* |
|---|---|---|---|
| *Region* | | | |
| PF | $1.71 \pm 0.10^{b}$ | $1.97 \pm 0.12^{a}$ | 21 |
| nPF | $5.42 \pm 0.47^{a}$ | $5.78 \pm 0.51^{a}$ | 9 |
| *Genus* | | | |
| *Larix* | $1.86 \pm 0.15^{b}$ | $2.44 \pm 0.21^{a}$ | 13 |
| *Picea* | $1.90 \pm 0.18^{a}$ | $2.05 \pm 0.20^{a}$ | 10 |
| *Pinus* | $5.64 \pm 0.64^{a}$ | $4.97 \pm 0.56^{b}$ | 7 |

**Table A.3**. Output of independent unit root tests for spatial synchrony ($\hat{a}_C$) and simple correlations ($r$) between aggregated tree-ring chronologies ($TRW_i$ BLUPs) at landscape type or genus level and summer (June–July) temperature. The unit root tests allowed for *drift* only or *drift* + *trend* in the time series depending on each particular group. The following statistics and associated probabilities are presented: the augmented Dickey-Fuller (ADF) τ statistic and the normalized bias $\rho$ statistic. Changes in both variables ($\hat{a}_C$ and $r$) are characterised for successive 30-year segments lagged by one year for the period 1911–1990.

| | **Spatial synchrony** | | | | | **$r$ ($TRW_i$ – June–July temp.)** | | | | |
|---|---|---|---|---|---|---|---|---|---|---|
| | | Normalised bias test | | ADF's $\tau$ | | | Normalised bias test | | ADF's $\tau$ | |
| | Type | $\rho$ | Prob. | $\tau$ | Prob. | Type | $\rho$ | Prob. | $\tau$ | Prob. |
| *Landscape* | | | | | | | | | | |
| PF | drift | -11.14 | 0.084 | -2.21 | 0.205 | drift + trend | -10.15 | 0.383 | -2.16 | 0.501 |
| nPF | drift + trend | -18.37 | 0.063 | -2.80 | 0.206 | drift + trend | -15.43 | 0.128 | -2.64 | 0.267 |
| *Genus* | | | | | | | | | | |
| *Larix* | drift + trend | -19.29 | 0.050 | -2.85 | 0.187 | drift + trend | -14.90 | 0.144 | -2.61 | 0.277 |
| *Picea* | drift + trend | -12.22 | 0.257 | -2.28 | 0.438 | drift + trend | -4.83 | 0.820 | -1.50 | 0.816 |
| *Pinus* | drift + trend | -14.30 | 0.165 | -2.64 | 0.264 | drift + trend | -20.08 | 0.041 | -3.01 | 0.139 |
| *Khanty-Mansiysk* | | | | | | | | | | |
| K-M[1] | drift + trend | -11.81 | 0.316 | -2.36 | 0.396 | drift + trend | -11.42 | 0.316 | -2.47 | 0.341 |

[1] Calculated over the period 1911–2013

**Figure A.1.** Flowchart showing the different steps followed to carry out the cointegration analysis applied to this work.

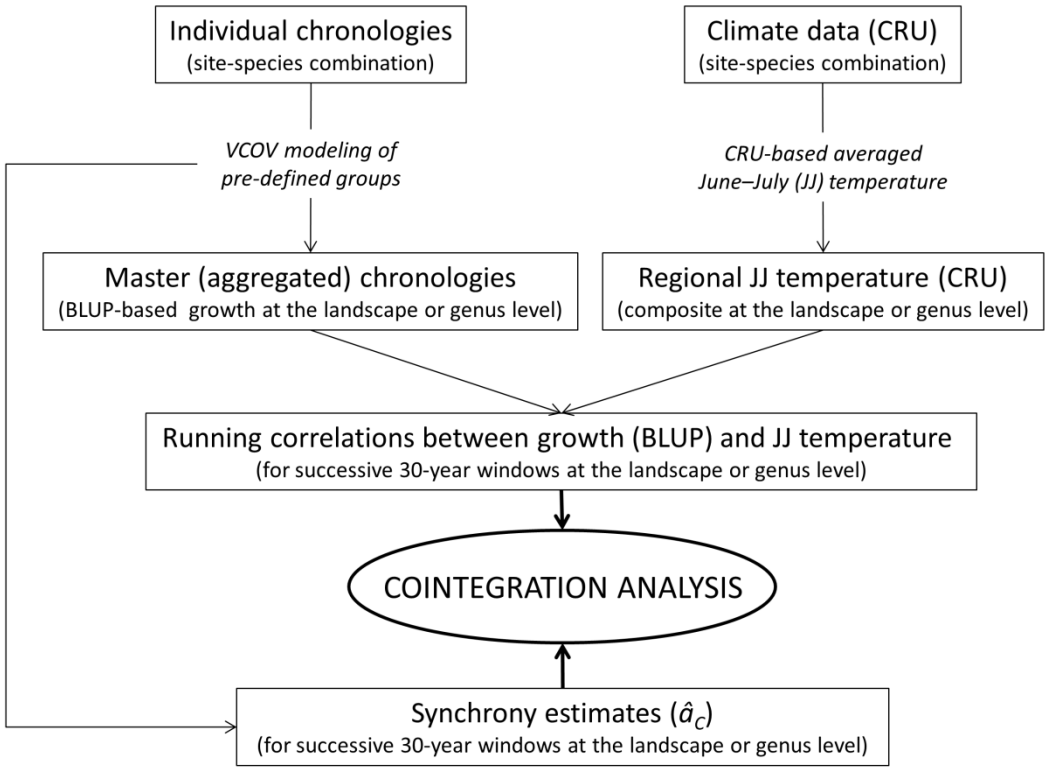

**Figure A.2.** Regional temporal trends in climate data for the study area for the period 1911–2013. Monthly long-term changes in **(a)** mean temperature and **(b)** precipitation derived from high-resolution (0.5° × 0.5°) CRU TS4.01 dataset (Harris *et al.*, 2014). Bars represent slopes of linear regression (*b*) of monthly climate factors as a function of time. Filled bars indicate significant linear trends over time ($P < 0.05$). Temporal evolution of **(c)** June–July temperature and **(d)** cold-season precipitation (PF = October to April; nPF = November to January). The trends (red lines) are smoothed by LOESS fitting (span = 0.2).

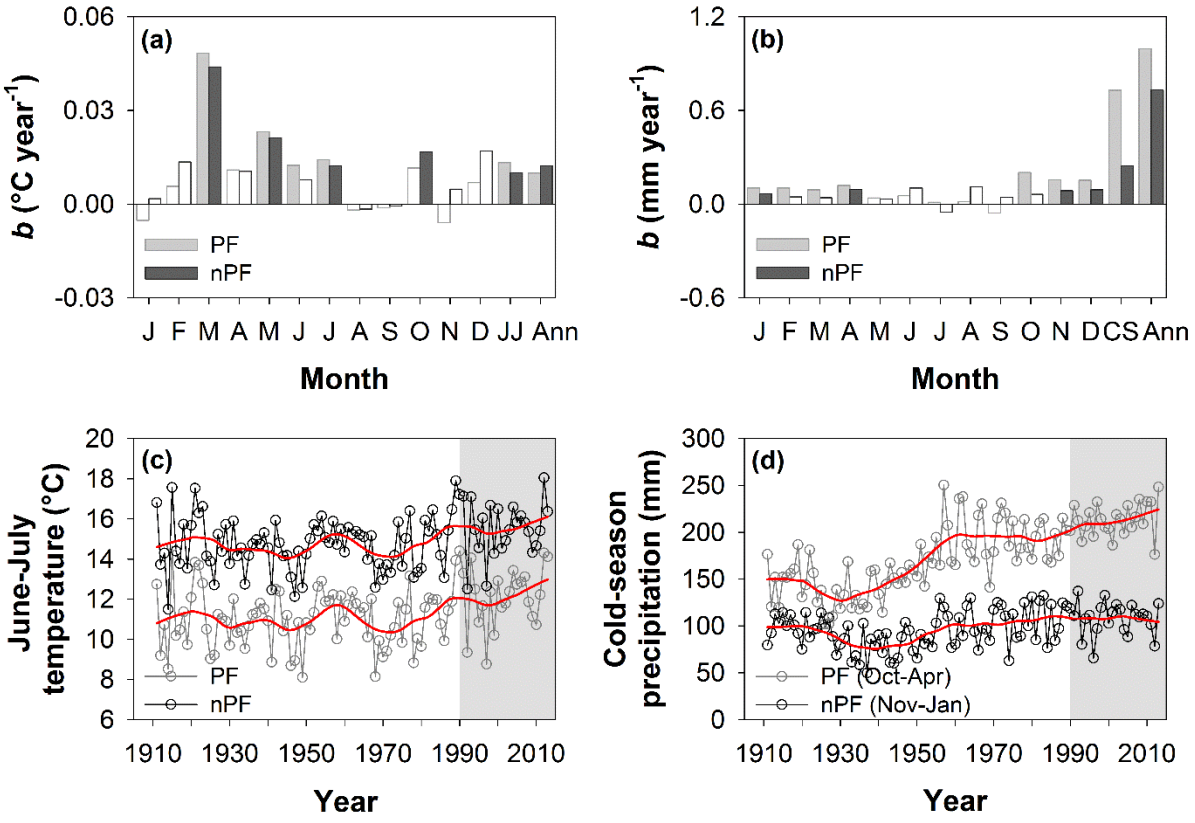

**Figure A.3.** Temporal changes in spatial synchrony ($\hat{a}_C$) at regional and genus levels for the set of updated Khanty-Mansiysk chronologies for the period 1911–2013. Changes in $\hat{a}_C$ were characterised for successive 30-year segments lagged by one year. Significant trends over time are depicted as Kendall's $\tau$ corresponding to the whole period. Asterisks after the $\tau$ values indicate level of significance: $^{***}P < 0.001$. Abbreviations: K-M, Khanty-Mansiysk; AB, *Abies*; PC, *Picea*; PI, *Pinus*.

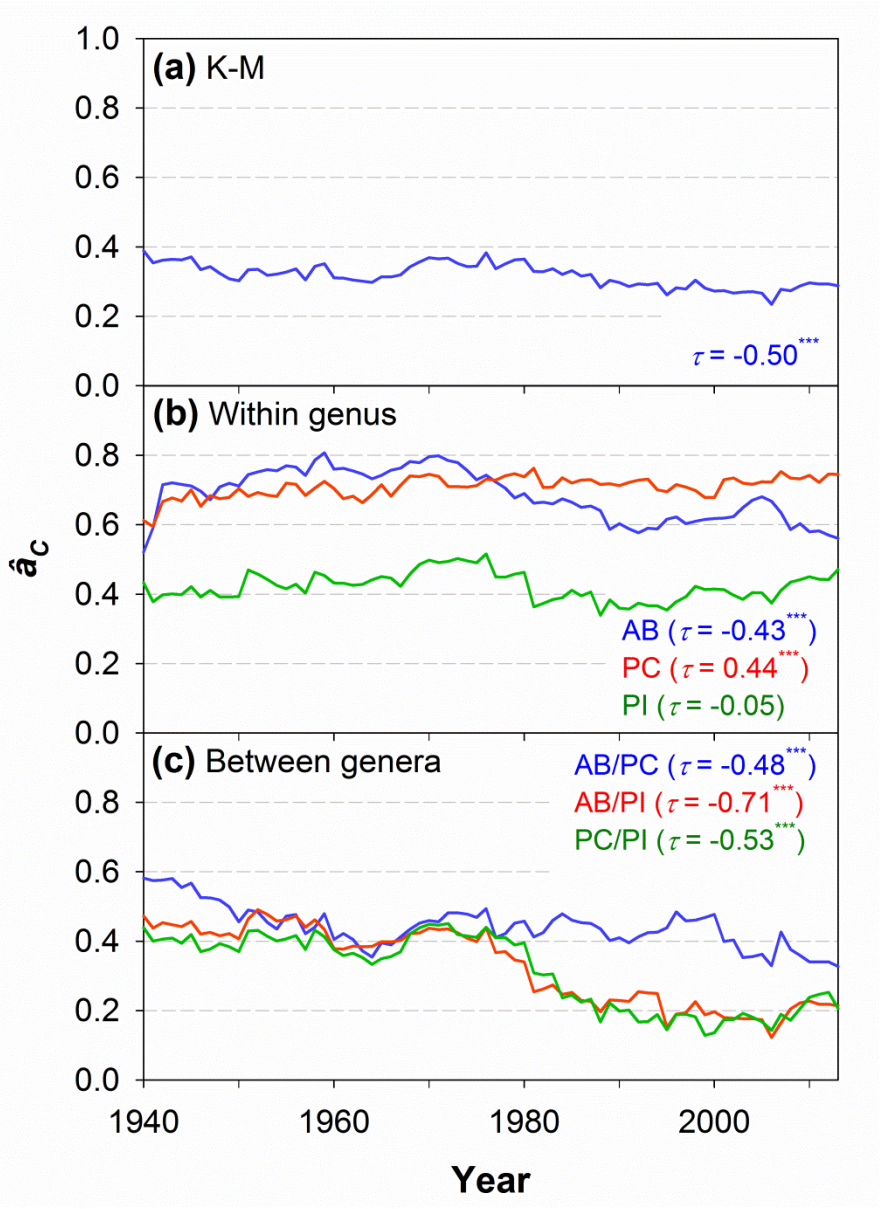

**Figure A.4.** Growth–climate associations at site level for the period 1911–1990. Tree responses to climate are based on bootstrapped correlations between individual indexed tree-ring chronologies ($TRW_i$) and **(a)** monthly mean temperature or **(b)** monthly precipitation. Green and orange colors denote positive and negative relationships, respectively. Only significant correlations ($P < 0.05$) are shown. Sites are sorted latitudinally, from north (top) to south (bottom). Lowercase and uppercase letters correspond to months of the years before and during tree-ring formation, respectively. Shaded area highlights summer (June–July) period of the current year.

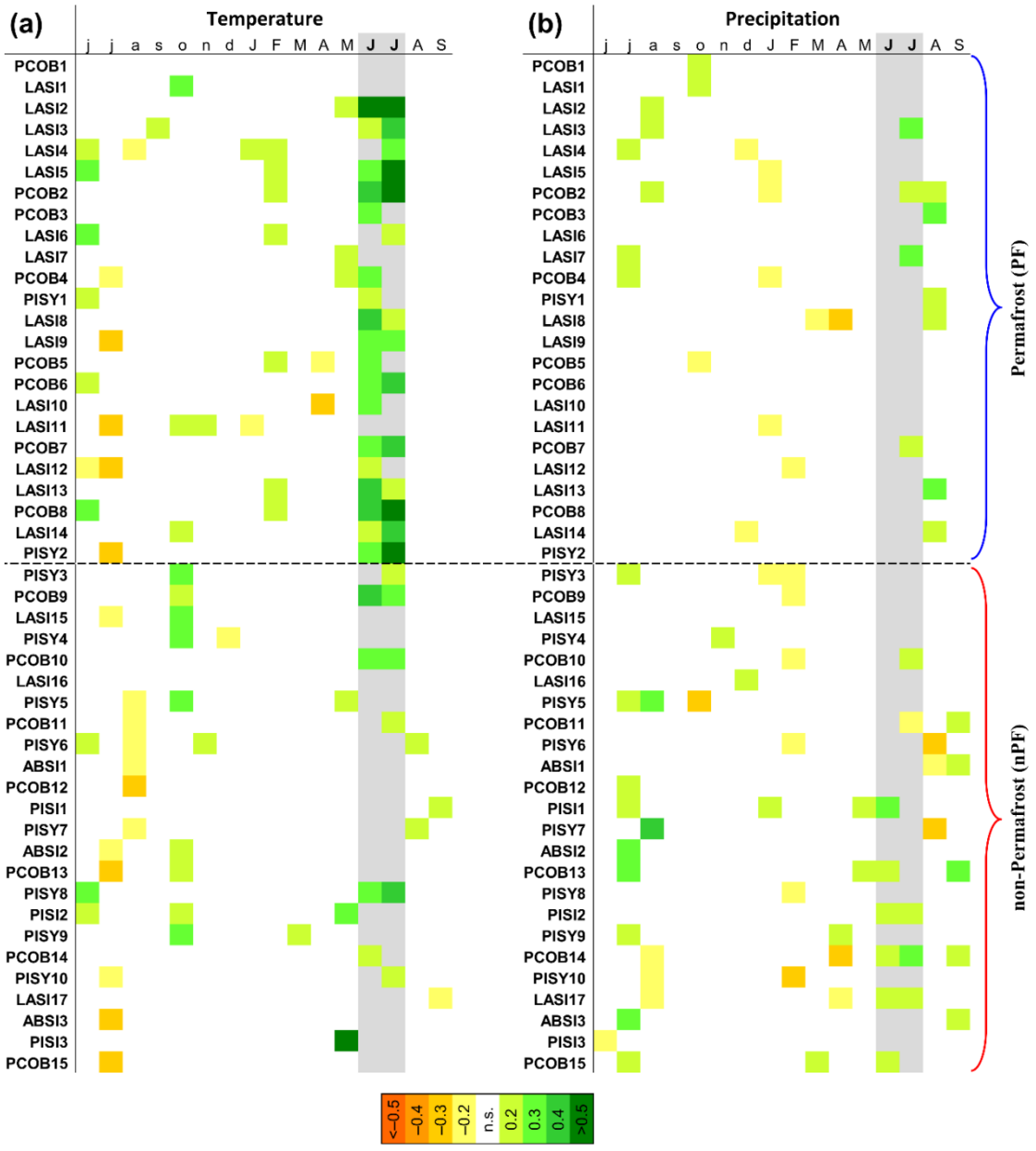

**Figure A.5.** Growth response to temperature records for the period 1911–1990: **(a)** permafrost (PF) and **(b)** non-permafrost (nPF). Tree responses to climate are based on bootstrapped correlations between regional master tree-ring chronologies (BLUPs) and either 'raw' (light grey) or residual climatic series (dark grey). The latter refers to temperature records after removing linear trend (if present) and first-order autocorrelation. The climate data are obtained from high-resolution (0.5° × 0.5°) CRU TS4.01 dataset (Harris *et al.*, 2014). Filled bars indicate significant correlations ($P < 0.05$). Lowercase and uppercase letters correspond to months of the years before and during tree-ring formation, respectively.

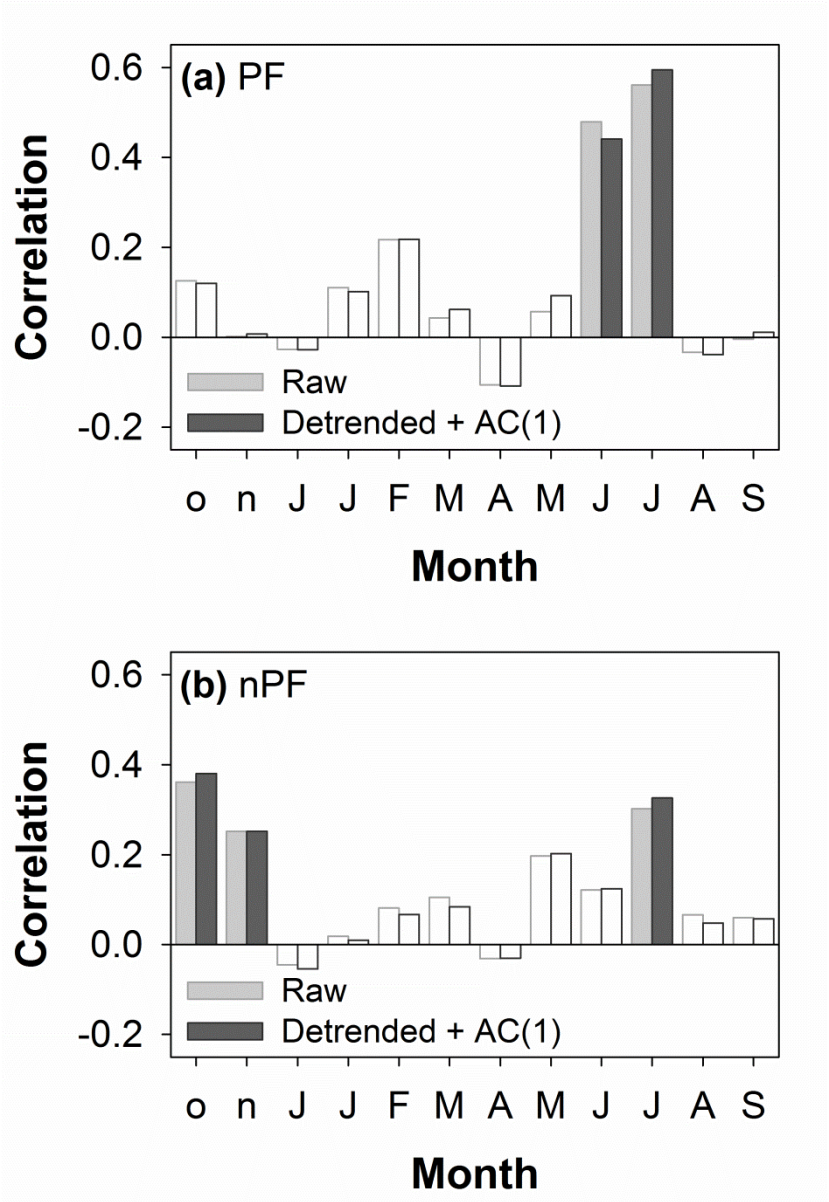

**Figure A.6.** Bootstrapped moving correlation analyses (*r*-values) between regional tree-ring width indices ($BLUP_{TRW}$) and June–July temperature ($T_{JJ}$) for successive 30-year segments lagged by one year independently for young (<200 years) and old (>200 years) chronologies: **(a)** permafrost (PF), and **(b)** non-permafrost (nPF). Significant correlations are depicted as filled symbols ($P < 0.05$). The standard errors of the estimates are shown as error bars. Years displayed on the *x*-axes correspond to the last year of 30-year moving intervals.

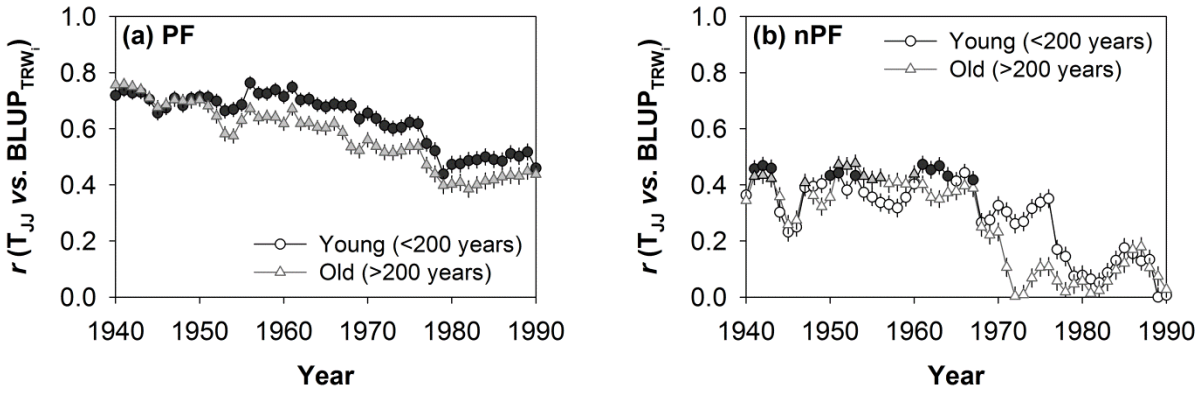

**Figure A.7.** Temporal changes in spatial synchrony ($\hat{a}_C$) of annual (blue lines) and summer (June–July; red lines) temperature records for the period 1911–2013. Synchrony estimates are calculated based on long-term local station data ($n = 7$). Changes in $\hat{a}_C$ were characterised for successive 30-year segments lagged by one year. Significant trends over time are depicted as Kendall's $\tau$ corresponding to the whole period Asterisks after the $\tau$ values indicate level of significance: $^{***}P < 0.001$.

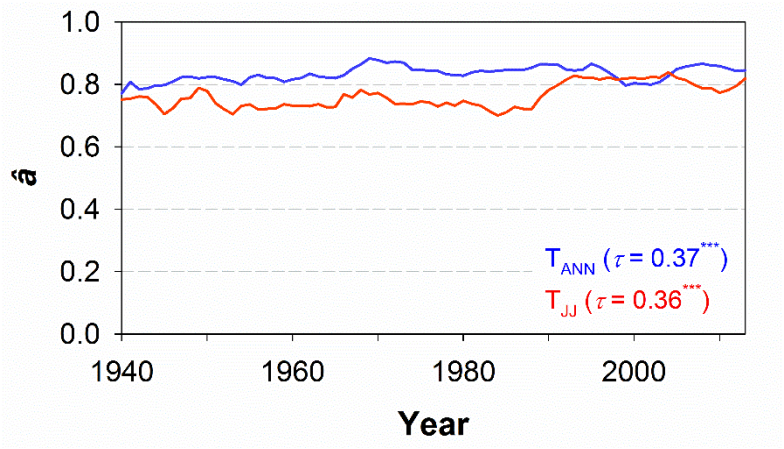

**Figure 1**

Click here to download high resolution image

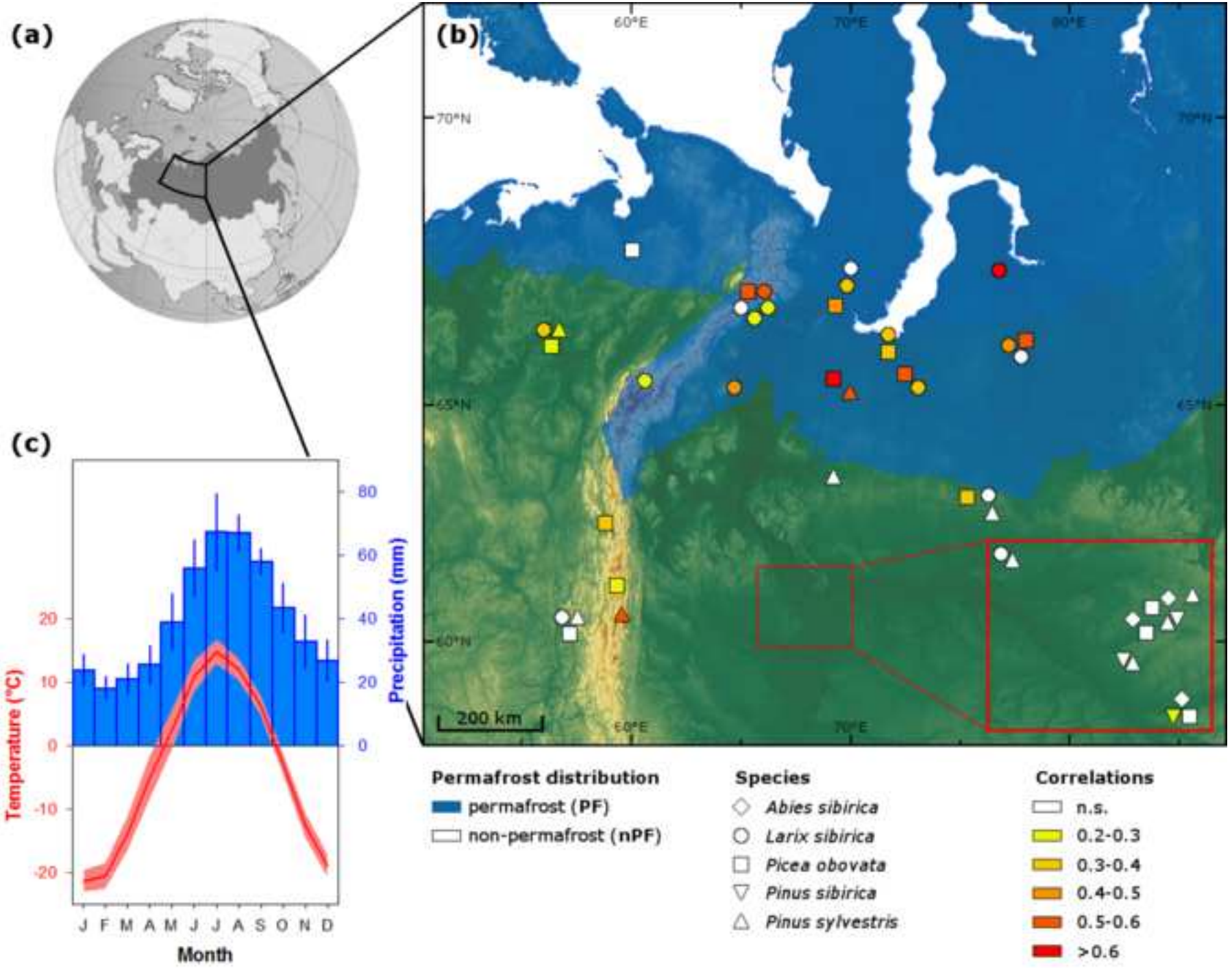

Figure 2

Click here to download high resolution image

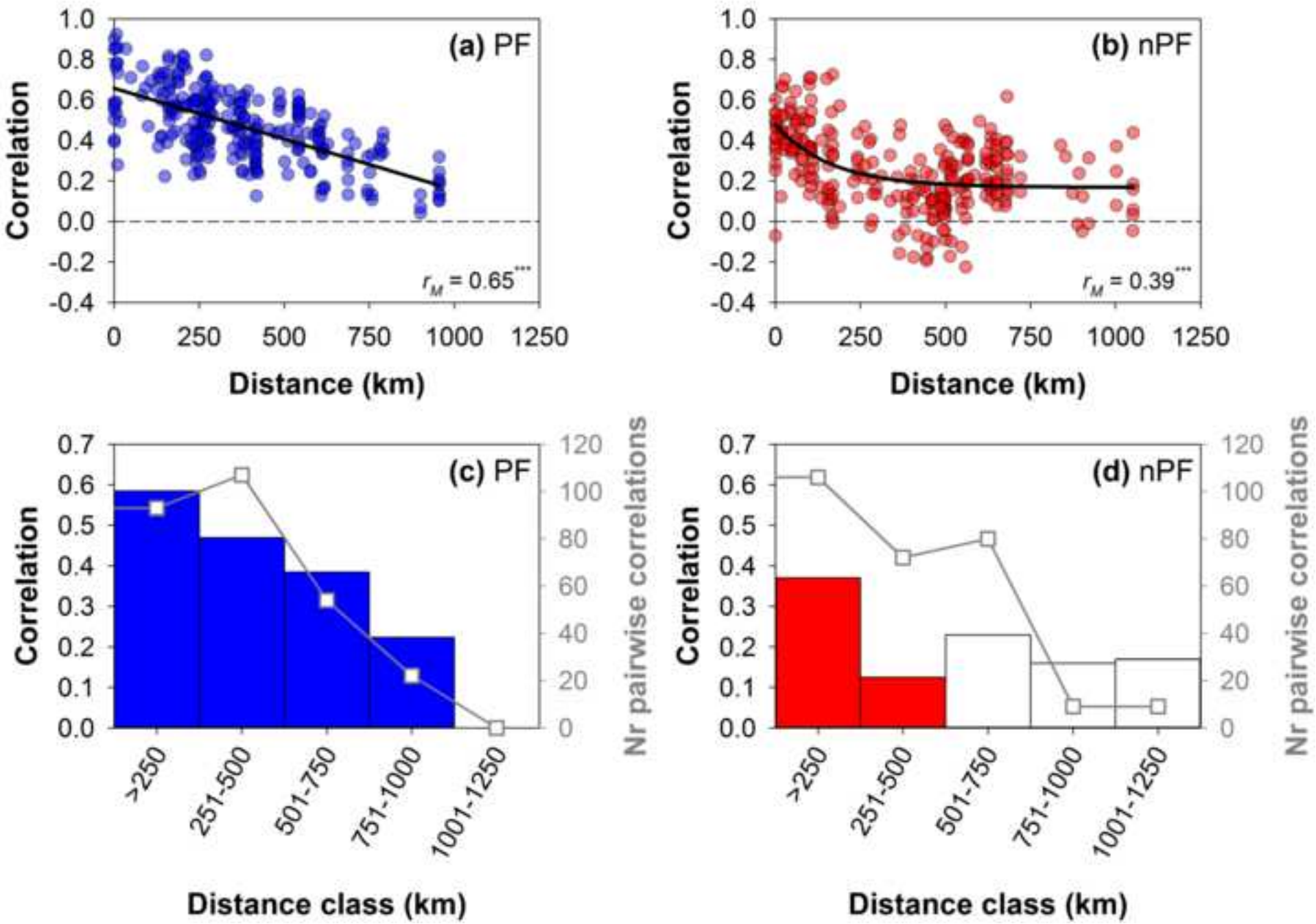

**Figure 3**

Click here to download high resolution image

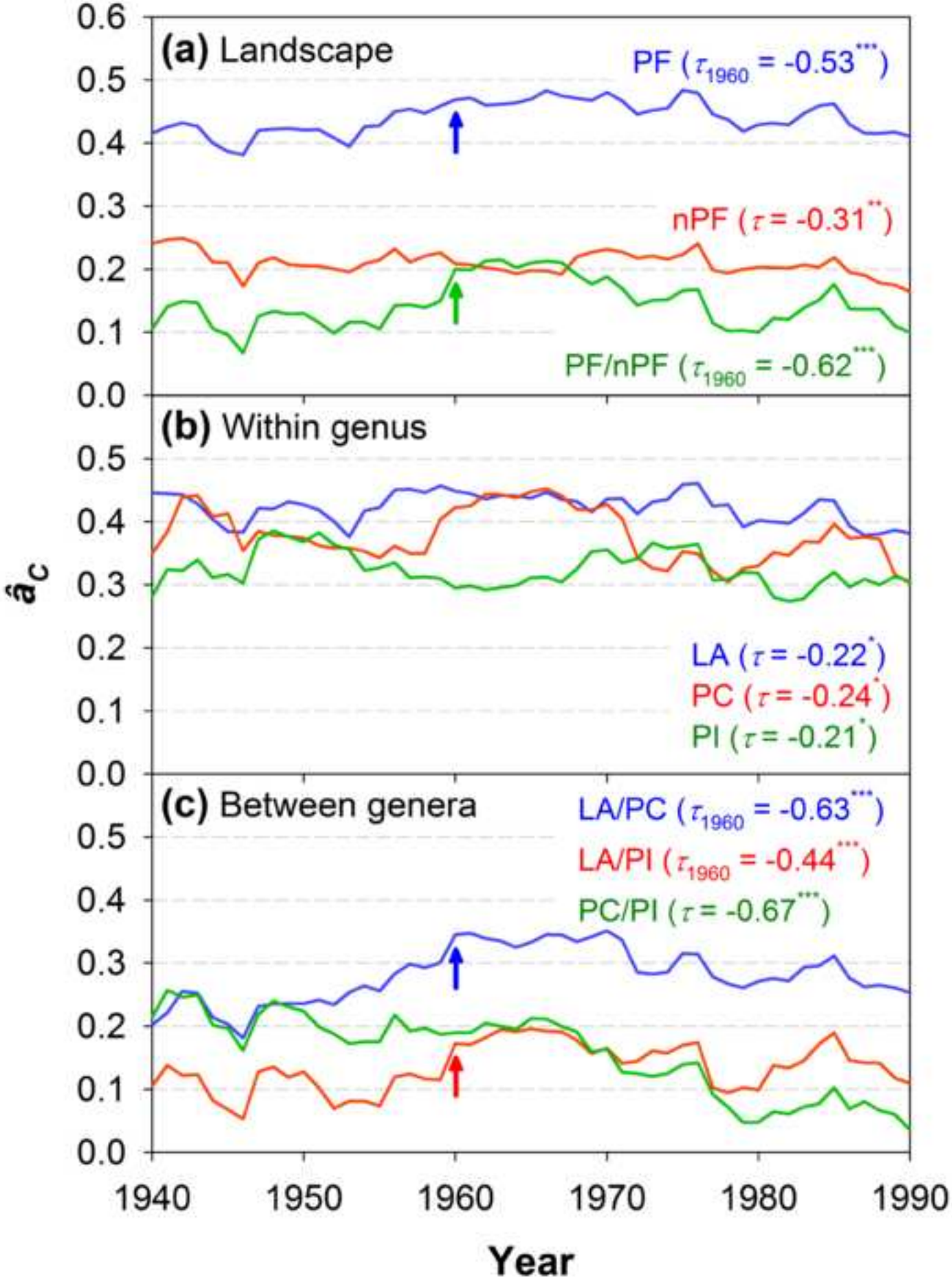

Figure 4

Click here to download high resolution image

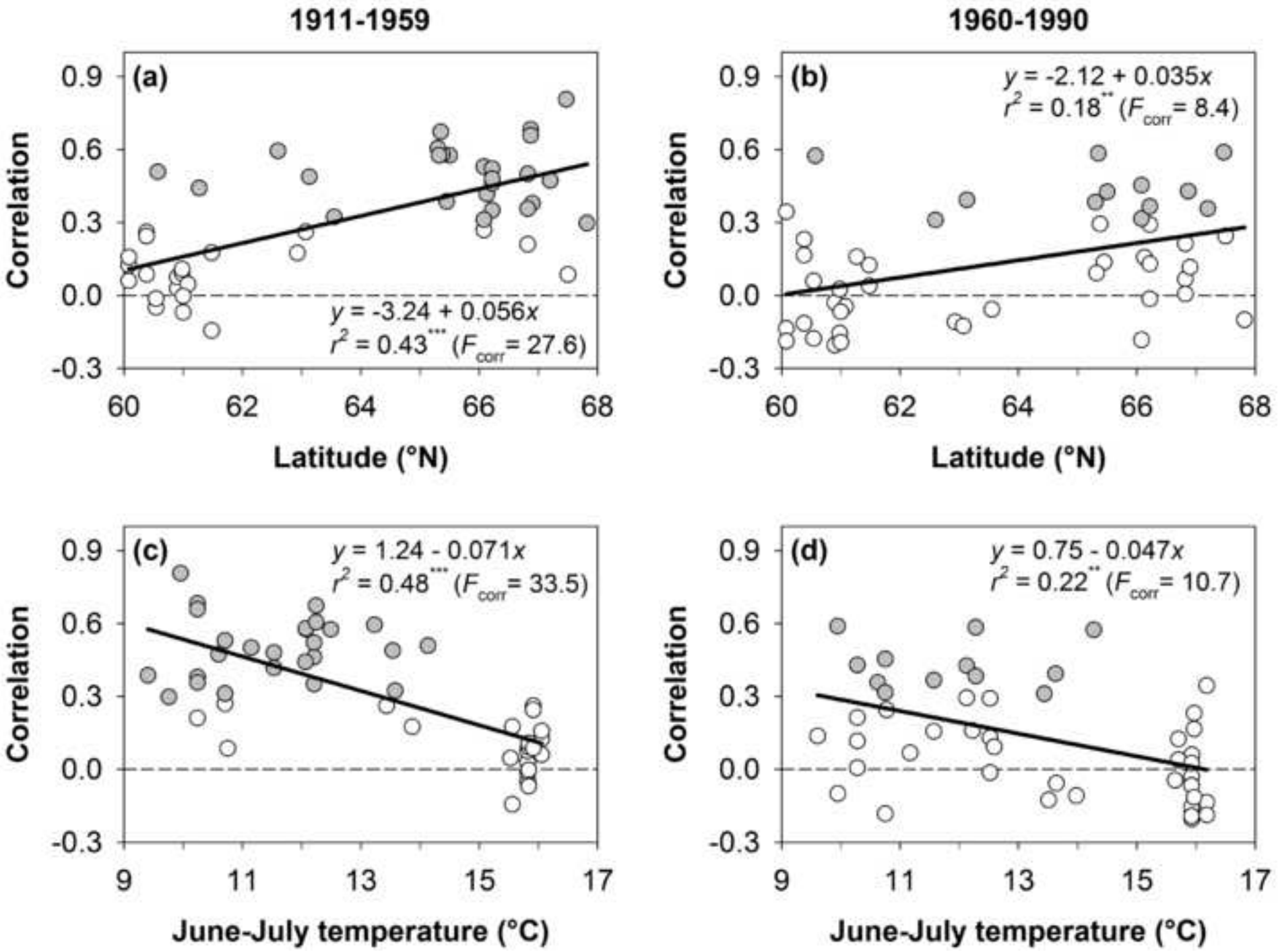

Figure 5

Click here to download high resolution image

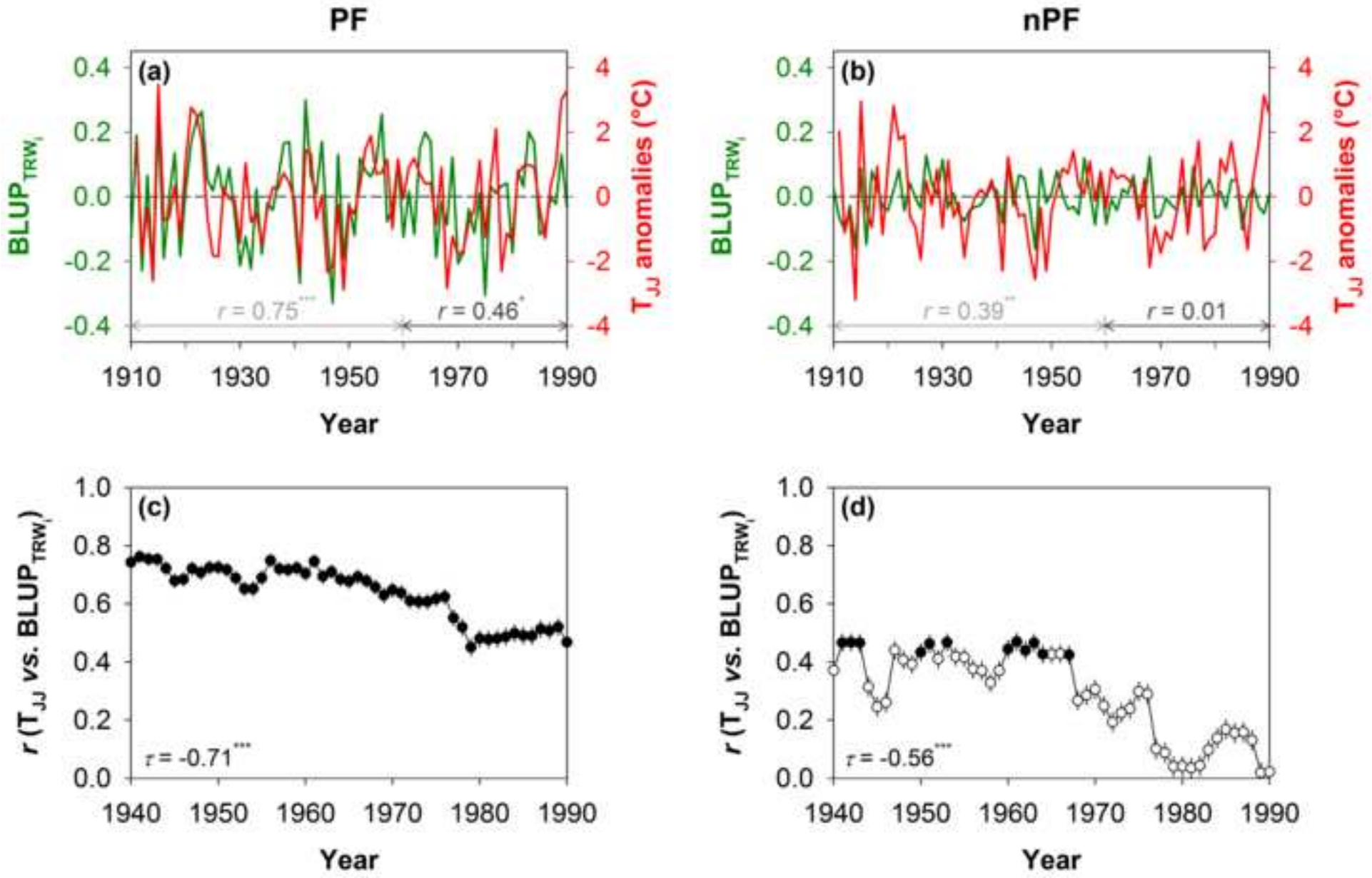

**Figure 6**

**Click here to download high resolution image**